Gauge Mediated Supersymmetry Breaking in a Next-to-Minimal Supersymmetric Model

Ellen Riefel

Department of Physics
Degree Project, 60 hp
Master's Programme in Theoretical Physics (120 hp)
Supervisor: Professor Sara Strandberg
Date: 14-10-2020

Stockholm University

Gauge Mediated Supersymmetry Breaking in a Next-to-Minimal Supersymmetric Model

Ellen Riefel

Abstract

This thesis can be divided into two main parts. The first part is concerned with a specific supersymmetric model and its theoretical foundation. First a general background to the Standard Model (SM) and the Minimal Supersymmetric Standard Model (MSSM) is given. After that a Next-to-Minimal Supersymmetric Standard Model (NMSSM) is introduced in which Supersymmetry is broken in three hidden sectors, solving the μ problem of the MSSM. The SUSY breaking is mediated by gauge bosons, introducing three additional neutralinos, which can decay into a lighter neutralino and a photon. The parameter space of this model is scanned and parameter values that could result in a detector signature with three photons and $E_{\mathrm{T}}^{\mathrm{miss}}$ in the final state are found and used to define a benchmark model. The second part of the thesis consists of a desription of the experimental work that is done to determine if the benchmark model could be detected with the ATLAS experiment at the LHC. First the data collection, simulation, reconstruction and selection in the ATLAS experiment is described. Then, using simulated data, the expected number of background events containing three photons and large $E_{\mathrm{T}}^{\mathrm{miss}}$ is estimated, as well as the expected number of signal events. An optimal set of selection criteria is determined by maximizing the discovery significance of the benchmark model. The largest discovery significance obtained is 17.5, which would allow for this model to be discovered. However, the estimate of the significance has large statistical uncertainties due to the limited number of simulated background events. Lastly, the sensitivity to the benchmark model of an excisting search is determined and found to not be large enough to allow for a discovery of the benchmark signal model.

Keywords: Supersymmetry, Next-to-Minimal Supersymmetric Model, Gauge Mediation, ATLAS, LHC

Acknowledgements

I would like to thank my supervisor Sara Standberg for her guidance during this project. Her help, patience and suggestions have been incredibly valuable to me and have benefited this thesis greatly. I would like to thank Gabriele Ferretti for his help with the theoretical part of this thesis and for the many things I have learned from him. Thanks to Diogo Buarque Franzosi for his contributions to finding the benchmark model.

Thanks to Michael, my family and my friends for always supporting and inspiring me.

Contents

Chapter 1

Introduction

The Standard Model (SM) is a theory that describes all the known elementary particles and three out of the four fundamental forces. Even though the predictions that the SM makes have been extensively tested and confirmed, there remain unsolved problems and unexplained phenomena. For example that the SM does not contain a viable candidate for Dark Matter, that it fails to include gravity and that it has a fine-tuning problem. These, among other things, hint towards physics beyond the SM.

One possibility to solve these problems is to extend the SM with Supersymmetry (SUSY) [1]. The lightest supersymmetric particle in SUSY could be a candidate for Dark Matter and introducing SUSY solves the fine-tuning problem. SUSY predicts that every fermion in the SM has a bosonic superpartner and vice versa. Besides the difference in spin of one half, these superpartner particles have the same quantum numbers as their SM-partners. Adding the most simple unconstrained supersymmetric extension to the SM gives the Minimal Supersymmetric Standard Model (MSSM) [1].

One way to find proof of SUSY is to detect these supersymmetric particles at the Large Hardron Collider (LHC) [2]. Unbroken SUSY would predict the masses of the supersymmetric particles to be the same as their SM counterparts. However just looking at chemistry rules out a supersymmetric partner of an electron with a mass of 0.511 MeV and other light masses of superparticles have been excluded similarly and with other experiments. This means that superpartners must be heavier than their SM counterparts and thus that SUSY must be broken.

SUSY can be broken in different ways, among which supergravity breaking [3] and Gauge Mediated Supersymmetry Breaking (GMSB). The latter is considered in this thesis. In GMSB SUSY is broken in one or more hidden sectors and the breaking is mediated to the visible spectrum by ordinairy gauge interactions [1].

If the supersymmetric particles are not too heavy, they could be hiding in the data that has been taken from hadron-hadron collisions at the LHC. The LHC experiments have been gathering data since 2009, but until this day there has not been found proof of the existence of SUSY.

This thesis consists of four chapters. The first chapter contains a brief introduction to the thesis. Chapter 2 provides the theoretical background necessary to understand the model that has been researched in this thesis. This includes a desription of the Standard Model (Section 2.1) and supersymmetry in general (Section 2.2). The model used as a benchmark model in this thesis is described in Section 2.3. Chapter 3 desribes the experimental part of this thesis. First the experimental setup of the ATLAS detector at the LHC is explained in Section 3.1, after which the process of data preparation and selection is decribed in Section 3.2. Sections 3.3 and 3.4 consist of information about the signal and background samples used in the analysis. In Section 3.5 the background is estimated and Section 3.6 contains the estimate for the signal events. The signal selection is optimized and the discovery significance is calculated in Section 3.7. Additionally, in Section 3.8, the sensitivity to the model in an existing search is determined. Finally, Chapter 4 contains a summary and conclusion of the work (Section 4.1) and an outlook (Section 4.2).

Chapter 2

Theoretical work

2.1 The Standard Model

The Standard Model is a very succesful theory that has been extensively tested and verified [4]. It describes all of the known elementary particles and three out of four fundamental forces.

2.1.1 Particles in the Standard Model

The particles in the Standard Model can be divided into two main groups, fermions and bosons.

Fermions have half-integer spin. They are divided into three generations where the particles in the lower generations are lighter than their counterparts in the higher generations. The particles in the first generation are stable as opposed to their counterparts in the second and third generation. Fermions can be divided into two groups; quarks and leptons. Quarks are affected by the strong, weak and electromagnetic forces. Two or more quarks bound together by the strong force form a so-called hadron. Leptons are affected by the weak and electromagnetic force, but not by the strong force. If a lepton is electrically charged it interacts with the electromagnetic and weak forces. A neutral lepton, called a neutrino, is on the other hand only affected by the weak force. Table 2.1 shows an overview of the fermions in the Standard Model.

	1st generation	2nd generation	3rd generation	charge
Quarks	up (u)	charm (c)	top (t)	$+\frac{2}{3}$
	down (d)	strange (s)	bottom (b)	$-\frac{1}{3}$
Leptons	electron (e)	muon (μ)	tau (τ)	-1
	electron neutrino (ν_e)	muon neutrino (ν_μ)	tau neutrino (ν_τ)	0

Table 2.1: The fermions in the Standard Model

Bosons are particles with integer spin. The gluon, photon, Z and W bosons are called gauge (or vector) bosons. These have spin = 1 and carry forces; the strong force is mediated by gluons and confines quarks into hadrons, the weak force is mediated by W and Z bosons and is responsible for radioactive decay and the electromagnetic force is mediated by photons and affects charged particles. The fourth fundamental force, gravity, is not included in the Standard Model. The most recent addition to the Standard Model is the Higgs particle. This is a scalar boson that has spin = 0 and was observed for the first time in 2012 at the LHC [5][6]. The bosons in the SM are summarized in Table 2.2.

	particle	charge	carried force
Gauge	gluon (g)	0	Strong force
	photon (γ)	0	Electromagnetic force
	Z boson (Z)	0	Weak force
	W boson ($W^\pm$)	± 1	Weak force
Scalar	Higgs (H)	0	

Table 2.2: The bosons in the Standard Model

2.1.2 Symmetry breaking

The particles in the Standard Model can be thought of as excitations of an underlying field in a quantum field theory. The interactions between particles are mediated by these fields. The fields can be described by a Lagrangian that often has a number of symmetries. According to Noether's theorem each

symmetry leads to a conserved quantity [7]. The Standard Model Lagrangian has symmetries that lead for example to the conservation of charge, energy and momentum.

These symmetries can be broken in two ways; explicitly and spontaneously. Under an explicitly broken symmetry the equations of motions are not invariant. Under a spontaneously broken symmetry the equations of motion are invariant, however the vacuum solutions of the equations of motion are not. Goldstone's theorem says that if a symmetry is broken spontaneously there must exist spinless particles of zero mass called Nambu-Goldstone bosons [8].

In the SM the Higgs field is responsible for spontaneously breaking the electroweak symmetry. Due to the Higgs mechanism [9, 10, 11] the would-be Goldstone bosons from this breaking are 'eaten' by the gauge bosons, giving the gauge bosons non-zero masses.

2.1.3 Problems of the Standard Model

Although the Standard Model has been extensively tested and verified, it cannot be a fundamental theory. There are phenomena that the SM does not predict or desribe, such as the baryon asymmetry in the universe [12], the fact that the SM does not include gravity, the lack of a candidate for dark matter and the Higgs fine tuning problem.

A fine-tuning problem in a theory implies that in order for the theory to agree with observations or make accurate predictions, very precise cancellations of large terms that contribute to a small parameter need to take place. The origin of these cancellations cannot be explained by the theory, which makes the theory less attractive.

Higgs fine-tuning problem
The Higgs field interacts with other particles giving them mass. It is a weak isospin doublet:

$$H = \frac{1}{\sqrt{2}} \begin{pmatrix} H_1 + iH_2 \\ H_3 + iH_4 \end{pmatrix} \tag{2.1}$$

The potential of the Higgs field is

$$V = m_H^2|H|^2 + \lambda|H|^4 \tag{2.2}$$

in which the parameters λ and m_H^2 (with the physical Higgs mass $M_H^2 = -2m_H^2$) contain contributions from interactions with other particles. For example the interaction of the Higgs field with a fermion with Yukawa coupling λ_f gives a correction

$$\Delta m_H^2 = -\frac{|\lambda_f|^2}{8\pi^2}\Lambda_{UF}^2 + ... \tag{2.3}$$

where Λ_{UF}^2 is an ultraviolet momentum cut-off used to regulate the loop integral [1]. Λ_{UF}^2 can be interpreted as the energy scale above which physics described by the Standard Model does not hold and new physics is needed.

The correction for the interaction of the Higgs field with a complex scalar particle S is

$$\Delta m_H^2 = \frac{\lambda_S}{16\pi^2}\Lambda_{UF}^2 - ... \tag{2.4}$$

As measured by the LHC experiments, the Higgs particle has a mass of approximately 125 GeV. The Standard Model requires a non-zero vacuum expectation value (VEV) for H ($\langle H \rangle$) at the minimum of the potential (Equation (2.2)), which occurs for $\lambda > 0$ and $m_H^2 < 0$. This leads to $\langle H \rangle = \sqrt{-m_H^2/\lambda}$.
By measuring properties of the weak interaction, it is known that $\langle H \rangle$ is approximately 246 GeV [4]. The measurement of the Higgs mass being approximately 125 GeV implies that $m_H^2 = -(92.9\text{GeV})^2$ and $\lambda = 0.126$ [1]. This means that the corrections to m_H^2 (Δm_H^2) need to be small. If Λ_{UF}^2 is taken to be the Planck scale at the order of 10^{31} GeV, the free parameters of the model need to be extremely fine-tuned or there must be some other reason that these and higher order corrections would cancel out in order to have a small Δm_H^2.

2.2 Supersymmetry

Supersymmetry (SUSY) is a theory that attempts to solve some of the problems that the Standard Model has. SUSY gives for instance a candidate for

dark matter and can solve the Higgs fine-tuning problem by introducing a new symmetry.

In supersymmetry the Standard Model is extended by introducing an additional symmetry between bosons and fermions, adding a so-called superpartner for each of the SM particles. The quantum numbers of these superpartners are the same as those of their SM counterparts with the exception of the spin, which differs by half a unit. Thus in SUSY a SM fermion has a bosonic superpartner and a SM boson has a fermionic superpartner.

Superpartners of SM fermions are named by adding an 's' in front of the name of their SM counterparts, for example the superpartner of a top-quark is called a 'stop' and the superpartner of a neutrino is called a sneutrino. Fermionic superpartners of bosons are named by adding 'ino' to the end of the name of their SM partners, so the superpartner of a Higgs boson is called a 'Higgsino' and that of a gluon is a 'gluino'. Superpartners are denoted with a tilde, for example the symbol of the superpartner of a SM W boson is $\tilde{W}$

Introducing SUSY means that there are two complex scalars with $\lambda_S = |\lambda_f|^2$ for every quark or lepton, so that the terms in Equations (2.3) and (2.4) cancel each other and similar cancellation happens for higher order terms. The cancellation is exact if SUSY is unbroken since $m_S = m_f$, otherwise, if SUSY is broken, the quadratic dependence on the cut-off is reduced to a logarithmic dependencce. This means that fine-tuning is no longer needed and SUSY therefore presents an elegant solution for the Higgs fine-tuning problem [1].

2.2.1 Supersymmetry breaking

If supersymmetry was unbroken, the superpartner particles would have the same masses as their SM counterparts. This can however be excluded directly, since there cannot exist a selectron of 0.511 MeV. The superparticles would furthermore have easily been detected by experiments like those at the LHC. Until this day there has been no hint towards the existence of these light superpartners, indicating particles with these characteristics and masses do not exist. This means that supersymmetry must be broken, causing superpartners to have higher masses than their SM partner particles,

explaining why they have not been seen in any experiment yet.

In order to maintain the solution that supersymmetry has to the Higgs fine-tuning problem, SUSY can only be broken in a way that lets the couplings obey $\lambda_S = |\lambda_f|^2$. So that the quadratic dependence on the cut-off scale in the radiative corrections to the Higgs mass (Equations (2.3) and (2.4)) are still reduced to logarithmic dependences. This can be achieved by introducing a soft SUSY breaking term to the Lagrangian:

$$\mathcal{L} = \mathcal{L}_{\text{SUSY}} + \mathcal{L}_{\text{soft}} \tag{2.5}$$

This additional term $\mathcal{L}_{\text{soft}}$ does not introduce quadratic divergences and can thus only contain mass terms and couplings with a positive mass dimension.

The origin of these soft breaking terms is unknown, but they can arise by introducing messengers that couple to the origin of the SUSY breaking sector (hidden sector) and mediate to the visible particles in a model like the Minimal Supersymmetric Standard Model (Section 2.2.4) (visible sector). Models in which this mediation is done through graviational-strength interactions are called Planck-scale-mediated SUSY breaking models, an example of this are supergravity models [13]. The model described in this thesis is a GMSB model. Models with gauge mediatied SUSY breaking can give a full, concrete and often fully calculable extension of the SM or MSSM [14].

2.2.2 Gauge Mediated Supersymmetry Breaking

In GMSB one or multiple additional chiral supermultiplets are introduced that function as the above-mentioned messengers and mediate between the SUSY breaking origin and the visible sector. These chiral supermultiplets are states of a so-called Spurion superfield. This superfield couples directly to the source of the SUSY breaking and indirectly to (s)quarks, (s)leptons and higgs(inos). The terms that this introduces to the superpotential do not introduce quadratic divergences. In gauge mediation the effects of gravity are subleading.

Typical theories have one Spurion Superfield, so SUSY breaking in one hidden sector, leading to one very light neutralino in addition to the ones from the visible sector. In this thesis a model is presented with SUSY breaking in three hidden sectors, leading to three extra neutralinos. This could

change the phenomenology significantly.

Each hidden sector or Spurion superfield provides a neutral fermion that can mix with the other neutral fermions to form mass eigenstates. The lightest of these mass eigenstates can be the lightest supersymmetric particle (LSP) and could be a candidate for dark matter.

2.2.3 SUSY Lagrangian and notation

The basic assumptions that are made about the supersymmetric model discussed in this thesis are that it has 4 dimensions, that it has one supersymmetry generator ($\mathcal{N} = 1$) and that gravity is not included. The generator Q generates the supersymmetric transformation:

$$Q|\text{Boson}\rangle = |\text{Fermion}\rangle \qquad Q|\text{Fermion}\rangle = |\text{Boson}\rangle \tag{2.6}$$

In supersymmetry algebra a SM particle and its superpartner each are a component in one so-called supermultiplet. These supermultiplets are irreducible representations of supersymmetry. The two supermultiplets used in this thesis are the chiral and gauge (or vector) supermultiplets. A chiral supermultiplet contains a two-component Weyl fermion and a complex scalar field. A gauge multiplet is a combination of a spin-$\frac{1}{2}$ gaugino and a spin-1 gauge boson. One could try to accomodate SM fermions in a gauge multiplet since they have spin $= \frac{1}{2}$, however this does not work, since their left-handed parts transform differently under gauge transformations than their right-handed parts. This can only be the case in a chiral supermultiplet. Additionally a gauge multiplet is always in the adjoint representation of the gauge group, while SM fermions are not.

Superfield notation offers a better way of seeing supersymmetry in contrast to the classical Lagrangian where supersymmetry is not manifested. The coordinates needed to describe so-called superspace in superfield notation are

$$x^\mu, \theta^\alpha, \theta^\dagger_{\dot{\alpha}} \tag{2.7}$$

where $\alpha, \dot{\alpha} = 1, 2,\ \mu = 1, .., 4$ and θ^α and $\theta^\dagger_{\dot{\alpha}}$ are constant complex anti-commuting two-component spinors with dimension $[\text{mass}]^{-\frac{1}{2}}$. Supersymme-

try is now a translation in superspace:

$$\begin{aligned} x^\mu &\to x^\mu + i\epsilon\sigma^\mu\theta^\dagger + i\epsilon^\dagger\bar{\sigma}^\mu\theta \\ \theta^\alpha &\to \theta^\alpha + \epsilon^\alpha \\ \theta^\dagger_{\dot{\alpha}} &\to \theta^\dagger_{\dot{\alpha}} + \epsilon^\dagger_{\dot{\alpha}} \end{aligned} \tag{2.8}$$

where $\sigma^0 = \left(\begin{smallmatrix} 1 & 0 \\ 0 & 1 \end{smallmatrix}\right)$, σ^i are the Pauli matrices and $\bar{\sigma}^\mu = (\sigma^0, -\sigma^i)$.

With the superspace coordinates in Equation (2.7) one can write down a general superfield S as an expansion in a power series in the anti-commuting variables θ^α and $\theta^\dagger_{\dot{\alpha}}$:

$$S(x,\theta,\theta^\dagger) = a + \theta\xi + \theta^\dagger\chi^\dagger + \theta\theta b + \theta^\dagger\theta^\dagger c + \theta^\dagger\bar{\sigma}^\mu\theta v_\mu + \theta^\dagger\theta^\dagger\theta\eta + \theta\theta\theta^\dagger\zeta^\dagger + \theta\theta\theta^\dagger\theta^\dagger d \tag{2.9}$$

in which the components are complex functions of x^μ; a, b, c, d and v_μ are 8 bosonic fields and $\xi, \chi^\dagger, \eta, \xi^\dagger$ are 4 two-component fermionic fields. Each term can at the most have two θ's and $\theta^\dagger$'s since they each have two independent components and are anti-commuting.

In order to obtain the mixing terms in mass matrices one needs to integrate the superfield. For this $d^2\theta$ and $d^2\theta^\dagger$ are defined as follows:

$$d^2\theta = -\frac{1}{4}d\theta^\alpha d\theta^\beta\epsilon_{\alpha\beta} \qquad\qquad d^2\theta^\dagger = -\frac{1}{4}d\theta^\dagger_{\dot{\alpha}} d\theta^\dagger_{\dot{\beta}}\epsilon^{\dot{\alpha}\dot{\beta}} \tag{2.10}$$

where $\epsilon_{\alpha\beta}, \epsilon^{\dot{\alpha}\dot{\beta}}$ is the antisymmetric symbol, so that

$$\int d^2\theta\ \theta\theta = 1 \qquad\qquad \int d^2\theta^\dagger\ \theta^\dagger\theta^\dagger = 1 \tag{2.11}$$

This means that integration over superspace of the general superfield in Equation (2.9) picks out the terms with the $\theta\theta$ or $\theta^\dagger\theta^\dagger$:

$$\int d^2\theta\ S(x,\theta,\theta^\dagger) = b(x) + \theta^\dagger\zeta^\dagger(x) + \theta^\dagger\theta^\dagger d(x) \tag{2.12}$$

$$\int d^2\theta^\dagger\ S(x,\theta,\theta^\dagger) = c(x) + \theta\eta(x) + \theta\theta d(x) \tag{2.13}$$

$$\int d^2\theta d^2\theta^\dagger\ S(x,\theta,\theta^\dagger) = d(x) \tag{2.14}$$

The chiral and vector superfields that describe the particles in the Standard Model can be obtained by putting constraints on the general superfield. To obtain a chiral superfield Φ and its complex conjugate Φ^*, an anti-chiral superfield, impose

$$\bar{D}_{\dot{\alpha}}\Phi = 0 \qquad\qquad D_\alpha \Phi^* = 0 \tag{2.15}$$

where

$$\bar{D}_{\dot{\alpha}} = -\frac{\partial}{\partial\theta^{\dagger\dot{\alpha}}} + i(\theta\sigma^\mu)_{\dot{\alpha}}\partial_\mu \qquad\qquad D_\alpha = \frac{\partial}{\partial\theta^\alpha} - i(\sigma^\mu\theta^\dagger)_\alpha\partial_\mu \tag{2.16}$$

are defined to be the chiral covariant derivatives. This results in the chiral superfields

$$\Phi = \phi + \sqrt{2}\theta\psi + \theta\theta F \tag{2.17}$$

$$\Phi^* = \phi^* + \sqrt{2}\theta^\dagger\psi^\dagger + \theta^\dagger\theta^\dagger F^* \tag{2.18}$$

where $\phi = \phi(y)$ is a complex scalar field, $\psi = \psi(y)$ a two-component vector field, $F = F(y)$ an auxiliary field and $y = x^\mu + i\theta^\dagger\bar{\sigma}^\mu\theta$. The $\sqrt{2}$ is a convention.

To obtain a vector superfield V the constraint $V = V^*$ is imposed or equivalently the constraints

$$a = a^* \qquad \chi^\dagger = \xi^\dagger \qquad c = b^* \qquad v_\mu = v_\mu^* \qquad \zeta^\dagger = \eta^\dagger \qquad d = d^* \tag{2.19}$$

are imposed on the general superfield Equation (2.9). Then the component expansion of the vector superfield can be written down and after applying the Wess-Zumino gauge to get rid of redundant degrees of freedom [15] the vector superfield becomes

$$V = \theta^\dagger\bar{\sigma}^\mu\theta A_\mu + \theta^\dagger\theta^\dagger\theta\lambda + \theta\theta\theta^\dagger\lambda^\dagger + \frac{1}{2}\theta\theta\theta^\dagger\theta^\dagger D \tag{2.20}$$

The Lagrangian density can be obtained by integrating the vector superfield in Equation (2.20) over superspace as in Equation (2.14). This gives the so-called D-term and contains the kinetic terms of the Lagrangian. Alternatively, one can note that if Φ is a chiral superfield, then $\Phi^*\Phi$ is a vector

superfield. Consequently, taking the $\theta\theta\theta^\dagger\theta^\dagger$ term of $\Phi^*\Phi$ also gives the D-term of the Lagrangian.

Another contribution to the Lagrangian density is obtained by integrating the $\theta\theta$ and $\theta^\dagger\theta^\dagger$ terms of a chiral superfield as in Equations (2.12) and (2.13). These contributions are called the F-terms and contain the mass and Yukawa interaction terms. Noting that any holomorphic function of chiral superfields also is a chiral superfield [1] the Lagrangian, without gauge interactions, can be written as

$$\mathcal{L}(x) = \int d^2\theta d^2\theta^\dagger \; \Phi^*\Phi + (\int d^2\theta \, W(\Phi) + c.c.) \tag{2.21}$$

where $W(\Phi)$ is any holomorphic function of the chiral superfields which corresponds to the superpotential. For $W = \frac{1}{2}M^{ij}\Phi_i\Phi_j + \frac{1}{6}y^{ijk}\Phi_i\Phi_j\Phi_k$ Equation (2.21) gives the full Lagrangian density. From this Lagrangian density the mixing and mass terms can be found. These can then be used to write down the mass matrices that are needed to calculate particle masses etc. Furthermore, the superfield equations of motion can be obtained from the Lagrangian density.

A special case of a chiral superfield is the Spurion superfield X introduced by gauge mediation (see Section 2.2.2). Since this field couples to the source of SUSY breaking, it must have a non-zero F-term and it thus generates the $\mathcal{L}_{\text{soft}}$ spontaneously. This Spurion field looks as follows

$$X = \sqrt{2}\theta\tilde{\eta} + \theta^2 F \tag{2.22}$$

where $F \neq 0$ and $\tilde{\eta}$ describes a neutral fermion [16].

2.2.4 Minimal Supersymmetric Standard Model

The Minimal Supersymmetric Standard Model (MSSM) is the minimal supersymmetric extension of the Standard Model. It contains chiral supermultiplets for the squarks/quarks $(Q, \bar{u}, \bar{d})$, sleptons/leptons $(L, \bar{e})$ and Higgs/Higgsinos (H_u, H_d) summarized in Table 2.3 and gauge multiplets for the gluino/gluon, wino/W bosons and bino/B boson summarized in Table 2.4 [1].

Names	spin 0	spin 1/2
Q	$(\tilde{u}_L\ \tilde{d}_L)$	$(u_L\ d_L)$
$\bar{u}$	$\tilde{u}_R^*$	$u_R^\dagger$
$\bar{d}$	$\tilde{d}_R^*$	$d_R^\dagger$
L	$(\tilde{\nu}\ \tilde{e}_L)$	$(\nu\ e_L)$
$\bar{e}$	$\tilde{e}_R^*$	$e_R^\dagger$
H_u	$(H_u^+\ H_u^0)$	$(\tilde{H}_u^+\ \tilde{H}_u^0)$
H_d	$(H_d^0\ H_d^-)$	$(\tilde{H}_d^0\ \tilde{H}_d^-)$

Table 2.3: Chiral supermultiplet content of the MSSM. The squarks/quarks and sleptons/leptons multiplets are only written for one family, but there are supermultiplets for all three families

spin 1/2	spin 1
$\tilde{g}$	g
$\tilde{W}^\pm\ \tilde{W}^0$	$W^\pm\ W^0$
$\tilde{B}^0$	B^0

Table 2.4: Gauge supermultiplet content of the MSSM

The gauge eigenstates can mix after electroweak symmetry breaking, resulting in mass eigenstates. Similarly the superpartners of the charged gauge bosons and Higgses can mix to form so-called charginos and the the superpartners of the neutral gauge bosons and Higgses can mix to form so-called neutralinos.

The superpotential of the MSSM is

$$W_{MSSM} = \bar{u}\boldsymbol{y_u}QH_u - \bar{d}\boldsymbol{y_d}QH_d - \bar{e}\boldsymbol{y_e}LH_d + \mu H_u H_d \tag{2.23}$$

where $H_u, H_d, Q, L, \bar{u}, \bar{d}, \bar{e}$ are the chiral superfields mentioned above and $\boldsymbol{y_u}, \boldsymbol{y_d}, \boldsymbol{y_e}$ are 3×3 matrices containing the dimensionless Yukawa couplings.

2.2.5 Problems of the MSSM

The last term in the superpotential of the MSSM (Equation (2.23)), $\mu H_u H_d$, is called the μ-term. This term determines the masses of the Higgsinos and contributes to the Higgs' self-interactions. In order for the VEV of the Higgs to be of the right order, the μ-term has to be of the order of the electroweak scale while the natural scale of this parameter would be the Planck scale or zero. This is called the μ problem.[17]

Furthermore there is a SUSY breaking counterpart of this μ-term in the soft SUSY breaking terms in the scalar potential $B\mu H_u H_d + h.c.$ [17]. Electroweak SUSY breaking implies that both μ and B must be around the electroweak scale, but there is no reason why these seemingly unrelated parameters should be so close to each other. This is referred to as the $\mu/B\mu$ problem [18].

2.2.6 Next-to-minimal Supersymmetric Standard Model

One solution to the μ and $\mu/B\mu$ problem is the introduction of a new gauge singlet to the MSSM. This supermultiplet can generate μ dynamically [19], meaning it does not have to be put in by hand like in the MSSM. This is the minimal extension of the MSSM, called the Next-to-Minimal Supersymmetric Standard Model (NMSSM). An additional reason to look at extensions of the MSSM is that there are phenomenological bounds that make it difficult to introduce gauge mediation to the MSSM [20], while in an extension this problem is mitigated.

Solution to the μ problem

In the NMSSM a new singlet field S is introduced. The μ term in the superpotential (given in Equation (2.23)) is then replaced by $\lambda S H_u H_d$. The S field has a VEV v_s and from this new term an effective μ term arises with $\mu_{\text{eff}} = \lambda v_s$ [21]. In this way the μ_{eff} parameter is determined by the soft SUSY breaking terms, giving a reason as to why the soft Higgs mass and μ are close together and of the electroweak scale, thus solving the μ problem.

The addition of this new gauge singlet in the NMSSM results in two more Higgs bosons and one additional neutral state called the singlino being added

to the contents of the MSSM. This singlino and the two additional Higgsinos can mix with the other gauginos and Higgsinos resulting in seven mass eigenstates of which five are neutral and two are charged. If there is CP-conservation in the Higgs boson sector, three of the neutral mass eigenstates are CP even and two are CP odd.

The masses and mixing of the particles in the NMSSM can be calculated starting from the NMSSM superpotential given by

$$W = \bar{u}\boldsymbol{y_u}QH_u - \bar{d}\boldsymbol{y_d}QH_d - \bar{e}\boldsymbol{y_e}LH_d + \lambda SH_uH_D + \frac{1}{3}\kappa S^3 \tag{2.24}$$

following the methods used in ref. [22].

2.3 Signal models

NMSSM models with gauge mediated SUSY breaking in one hidden sector have been studied [23, 24, 25], but no hint towards these models being realized in nature has been found at the LHC. This motivates studying modified or extended variations of these models.

SUSY breaking in one hidden sector is the usual GMSB model in the NMSSM. This model can be modified significantly by assuming that SUSY is broken in n ($n > 1$) hidden sectors, resulting in n neutralinos added to the five neutralinos from the visible sector. The lightest of these additional neutralinos becomes the usual (nearly massless) Goldstino of $n = 1$ models. The other additional neutralinos could give potentially interesting signatures that cannot be produced by $n = 1$ models or weaken the usual signatures of a model with one hidden sector.

The model studied in this thesis is limited to SUSY breaking in $n = 3$ hidden sectors and only electroweak production diagrams are considered. The SUSY breaking in three hidden sectors can result in a signature of three photons and missing transverse energy ($E_{\mathrm{T}}^{\mathrm{miss}}$). This signature is only very rarely produced by the SM and there has not been any search for it in ATLAS, so possible SUSY models that abundantly produce this signature might not have been discovered with the current searches. There have been studies focused on models with two hidden sectors and GMSB (Refs. [26], [27],

[28]), these mostly do not result in a three photon and $E_{\mathrm{T}}^{\mathrm{miss}}$ signature. In Ref. [16] models with multiple SUSY breaking sectors have been studied in the context of the MSSM and slepton pair production. Looking at models with multiple SUSY breaking sectors in the NMSSM could result in different phenomenology, since the singlino can mix with the other gauginos, resulting in a possible singlino-like neutralino as the LSP.

2.3.1 Particle content

There are seven Higgs bosons and five neutralinos present in the NMSSM (see Section 2.2.6). By introducing gauge mediated SUSY breaking in three hidden sectors, three more gauginos ($\tilde{\eta}_1, \tilde{\eta}_2, \tilde{\eta}_3$) that reside in the Spurion superfields are added. These gauginos mix with the EW gauginos ($\tilde{B}^0, \tilde{W}^0$), neutral higgsinos ($\tilde{H}_d^0, \tilde{H}_u^0$) and singlino ($\tilde{S}$) forming eight neutralino mass eigenstates ($\tilde{\chi}_1^0, ..., \tilde{\chi}_8^0$), where $\tilde{\chi}_1^0$ is the lightest and $\tilde{\chi}_8^0$ the heaviest. An overview can be found in Table 2.5 [22]. The squark, slepton and gluino content stays the same as in the MSSM, described in Table 2.3.

	gauge eigenstates	mass eigenstates
Higgs bosons	h_d, h_u, h_s, a, a_s	H_1, H_2, H_3, H_4, H_5 $(H_1, H_2, H_3, A_1, A_2)$
	H_d^-, H_u^+	$H^\pm$
neutralinos	$\tilde{B}^0, \tilde{W}^0, \tilde{H}_u^0, \tilde{H}_d^0, \tilde{S}, \tilde{\eta}_1, \tilde{\eta}_2, \tilde{\eta}_3$	$\tilde{\chi}_1^0, \tilde{\chi}_2^0, \tilde{\chi}_3^0, \tilde{\chi}_4^0, \tilde{\chi}_5^0, \tilde{\chi}_6^0, \tilde{\chi}_7^0, \tilde{\chi}_8^0$
charginos	$\tilde{W}^\pm, \tilde{H}_d^-, \tilde{H}_u^+$	$\tilde{\chi}_1^\pm, \tilde{\chi}_2^\pm$

Table 2.5: The Higgs bosons, neutralinos and charginos in the NMSSM. In case of CP conservation, the Higgs bosons mix to the mass eigenstates described in the brackets. H_1, H_2 and H_3 are CP odd and A_1 and A_2 are CP even.

2.3.2 Neutralino mass spectrum

The neutralino mass matrix $\mathcal{M}_{\tilde{\chi}^0}$ looks as follows in the eigenbasis $\psi^0 = \{\tilde{B}^0, \tilde{W}^{(3)}, \tilde{H}_d^0, \tilde{H}_u^0, \tilde{S}, \tilde{\eta}_1, \tilde{\eta}_2, \tilde{\eta}_3\}$

$$\mathcal{M}_{\tilde{\chi}^0} = \begin{pmatrix} M_{5\mathrm{x}5}^{\mathrm{nmssm}} & M_{5\mathrm{x}3}^{\mathrm{mix}} \\ M_{3\mathrm{x}5}^{\mathrm{mix}} & M_{3\mathrm{x}3}^{\tilde{\eta}} \end{pmatrix} \tag{2.25}$$

where M_{5x5}^{nmssm} is the 5×5 NMSSM mass matrix obtained as decribed in reference [22]:

$$M_{5x5}^{NMSSM} = \begin{pmatrix} M_B & 0 & -m_z s\theta c\beta & m_z s\theta s\beta & 0 \\ 0 & M_W & m_z c\theta c\beta & -m_z c\theta s\beta & 0 \\ -m_z s\theta c\beta & m_z c\theta c\beta & 0 & -\frac{\lambda v_s}{\sqrt{2}} & -\frac{\lambda v_u}{\sqrt{2}} \\ m_z s\theta s\beta & -m_z c\theta s\beta & -\frac{\lambda v_s}{\sqrt{2}} & 0 & -\frac{\lambda v_d}{\sqrt{2}} \\ 0 & 0 & -\frac{\lambda v_u}{\sqrt{2}} & -\frac{\lambda v_d}{\sqrt{2}} & \sqrt{2}\kappa v_s \end{pmatrix} \quad (2.26)$$

with abbreviations $s\theta = \sin\theta, c\theta = \cos\theta$ and θ the Weinberg angle. Since the soft masses get contributions from the three hidden breaking sectors, they can be written as

$$M_B = \sum_{i=1}^{3} M_{B(i)} \quad M_W = \sum_{i=1}^{3} M_{W(i)} \quad m_{H_{u/d}}^2 = \sum_{i=1}^{3} m_{H_{u/d}(i)}^2 \quad m_S^2 = \sum_{i=1}^{3} m_{S(i)}^2 \quad (2.27)$$

The VEVs for the Higgs fields, v_u and v_d, are related to the mass of the Z^0 boson and the electroweak gauge couplings [1]:

$$v_u^2 + v_d^2 = v^2 = 4m_Z^2/(g_1^2 + g_2^2) \approx (246\text{GeV})^2 \quad (2.28)$$

and as conventionally the ratio of the VEVs is written as $\tan\beta \equiv v_u/v_d$.

M_{5x3}^{mix} are the mixing terms of the three $\tilde{\eta}$'s with the gauginos from the NMSSM. These can be obtained by looking at all possible normalizable integrals, see Appendix A.

$$M_{5x3}^{mix} = \begin{pmatrix} -\frac{D_Y M_{B(1)}}{\sqrt{2}f_1} & -\frac{D_Y M_{B(2)}}{\sqrt{2}f_2} & -\frac{D_Y M_{B(3)}}{\sqrt{2}f_3} \\ -\frac{D_T^3 M_{W(1)}}{\sqrt{2}f_1} & -\frac{D_T^3 M_{W(2)}}{\sqrt{2}f_2} & -\frac{D_T^3 M_{W(3)}}{\sqrt{2}f_3} \\ \frac{-\sqrt{2}m_{H_d(1)}^2 v_d + \lambda A_{\lambda(1)} v_s v_u}{2f_1} & \frac{-\sqrt{2}m_{H_d(2)}^2 v_d + \lambda A_{\lambda(2)} v_s v_u}{2f_2} & \frac{-\sqrt{2}m_{H_d(3)}^2 v_d + \lambda A_{\lambda(3)} v_s v_u}{2f_3} \\ \frac{-\sqrt{2}m_{H_u(1)}^2 v_u + \lambda A_{\lambda(1)} v_s v_d}{2f_1} & \frac{-\sqrt{2}m_{H_u(2)}^2 v_u + \lambda A_{\lambda(2)} v_s v_d}{2f_2} & \frac{-\sqrt{2}m_{H_u(3)}^2 v_u + \lambda A_{\lambda(3)} v_s v_d}{2f_3} \\ -\frac{\sqrt{2}m_{S(1)}^2 v_s + \kappa A_{\kappa(1)} v_s^2 - \lambda A_{\lambda(1)} v_d v_u}{2f_1} & -\frac{\sqrt{2}m_{S(2)}^2 v_s + \kappa A_{\kappa(2)} v_s^2 - \lambda A_{\lambda(2)} v_d v_u}{2f_2} & -\frac{\sqrt{2}m_{S(3)}^2 v_s + \kappa A_{\kappa(3)} v_s^2 - \lambda A_{\lambda(3)} v_d v_u}{2f_3} \end{pmatrix} \quad (2.29)$$

The last contribution to $\mathcal{M}_{\tilde{\chi}^0}$ is the mass block $M^{\tilde{\eta}}_{3\text{x}3}$. The masses of the $\tilde{\eta}_i$'s get contributions from the renormalizable integrals (see Appendix A) and through radiative corrections. The contributions of the integrals are suppressed by a factor $\frac{1}{f_i^2}$, where f_i are the SUSY breaking scales, and are negligible. The second contribution strongly depends on the model, but using that SUSY is spontaneously broken, a general structure of $M^{\eta}_{3\text{x}3}$ can be determined as described below.

The mass matrix $\mathcal{M}_{\tilde{\chi}^0}$ has an eigenstate with a zero eigenvector corresponding to the lightest neutralino, which is approximately massless. The f_i are assumed to be much bigger than the VEVs of auxiliary D- and F-terms of the gauge and Higgs superfields. In this case the lightest neutralino will approximately be a linear combination of only the $\tilde{\eta}$'s. Since this linear combination forms a zero eigenvector of $M^{\tilde{\eta}}_{3\text{x}3}$, n conditions are put on this matrix. This leads to the possibility to express the diagonal entries of $M^{\eta}_{3\text{x}3}$ in terms of the off-diagonal entries $\mathcal{M}_{ij}(i < j)$. These off-diagonal entries are unknown and depend on the model [16]. Then $M^{\eta}_{3\text{x}3}$ will be structured as follows:

$$M^{\tilde{\eta}}_{3\text{x}3} = \begin{pmatrix} -\frac{f_2\mathcal{M}_{12}+f_3\mathcal{M}_{13}}{f_1} & \mathcal{M}_{12} & \mathcal{M}_{13} \\ \mathcal{M}_{12} & -\frac{f_1\mathcal{M}_{12}+f_3\mathcal{M}_{23}}{f_2} & \mathcal{M}_{23} \\ \mathcal{M}_{13} & \mathcal{M}_{23} & -\frac{f_1\mathcal{M}_{13}+f_2\mathcal{M}_{23}}{f_3} \end{pmatrix} \tag{2.30}$$

The mass eigenstates of the neutralinos can be calculated by diagonalizing the mass matrix $\mathcal{M}_{\tilde{\chi}^0}$ by a unitary matrix $\mathbf{U}$:

$$\tilde{\chi}^0_i = U_{ij}\tilde{\psi}^0_j \tag{2.31}$$

with $i, j = 1, .., 8$ so that

$$\mathbf{U}^*\mathcal{M}_{\tilde{\chi}^0}\mathbf{U}^\dagger = \text{diag}(m^2_{\tilde{\chi}^0_1}, m^2_{\tilde{\chi}^0_2}, m^2_{\tilde{\chi}^0_3}, m^2_{\tilde{\chi}^0_4}, m^2_{\tilde{\chi}^0_5}, m^2_{\tilde{\chi}^0_6}, m^2_{\tilde{\chi}^0_7}, m^2_{\tilde{\chi}^0_8}) \tag{2.32}$$

2.3.3 Model parameters

For certain choices of the parameters of the model the neutralinos can decay to a lighter neutralino and photon, which could result in a three photon and $E_{\text{T}}^{\text{miss}}$ signature. The following free parameters

$$\lambda,\ \kappa,\ \tan\beta,\ v_s,\ A_{\lambda(i)},\ A_{\kappa(i)}$$
$$M_{B(i)},\ M_{W(i)},\ f_i,\ \mathcal{M}_{12},\ \mathcal{M}_{13},\ \mathcal{M}_{23}$$

with $i = 1, 2, 3$ were scanned in Mathematica [29] to find combinations resulting in a three photon and $E_{\mathrm{T}}^{\mathrm{miss}}$ signature. In addition to giving the right masses and couplings to make a three photon and $E_{\mathrm{T}}^{\mathrm{miss}}$ signature possible, the set of parameters should also give a Higgs mass of 125 GeV, should obey the tadpole conditions [30] and should not give chargini or additional Higgs bosons that are too light so that they would have been detected in experiments already. First the parameters that appear in the bosonic mass matrices, $\lambda, \kappa, \tan\beta, v_s, A_{\lambda(i)}, A_{\kappa(i)}, M_{B(i)}$ and $M_{W(i)}$, that meet these requirements are found. After those parameters have been fixed, the rest of the parameters can be found.

In order to simplify the model and decrease the time needed to scan the parameter space the following simplifying assumptions have been made:

$$M_{B(i)} = x_i M_B \quad M_{W(i)} = x_i M_W$$
$$m^2_{H_d(i)} = x_i m^2_{H_d} \quad m^2_{H_u(i)} = x_i m^2_{H_u} \quad m^2_{S(i)} = x_i m^2_S$$
$$A_{\lambda(i)} = x_i A_\lambda \quad A_{\kappa(i)} = x_i A_\kappa$$
$$\mathcal{M}_{12} = \mathcal{M}_{13} = \mathcal{M}_{23} = \mathcal{M}$$

Thus the parameter $M_{B(i)}$ has been traded for $x_i M_B$ and similarly for the other parameters, reducing the number of parameters from 31 to 18. The following SM constants have been used:

$$G_f = 1.1663787 \times 10^{-5}\,\mathrm{GeV}^{-2},\ m_Z = 91.1876\,\mathrm{GeV},\ m_W = 80.379\,\mathrm{GeV}$$

where G_f is the Fermi coupling constant, m_Z the mass of the Z boson and m_W the mass of the W boson. From these parameters all other SM parameters can be calculated (see Appendix B).
For all parameter sets that satisfy the conditions listed above, the cross section (CS) and branching ratios (BR) are calculated with Madgraph [31].

The parameter set with the largest CS times BR to a three photon and $E_{\mathrm{T}}^{\mathrm{miss}}$ signature is

$$M_B = 300\,\mathrm{GeV},\ M_W = 800\,\mathrm{GeV}$$
$$x_1 = x_2 = x_3 = \frac{1}{3}$$
$$f_1 = 100,000\,\mathrm{GeV},\ f_2 = 10,000\,\mathrm{GeV},\ f_3 = 10,000\,\mathrm{GeV}$$
$$\mathcal{M} = 10\,\mathrm{GeV},\ \lambda = 3,\ \kappa = 0.529662,\ tan\beta = 1,\ v_s = 258.562\,\mathrm{GeV}$$
$$A_\lambda = 512.14\,\mathrm{GeV},\ A_\kappa = 31.7872\,\mathrm{GeV}$$

This is chosen as the benchmark model used in the remainder of this thesis.

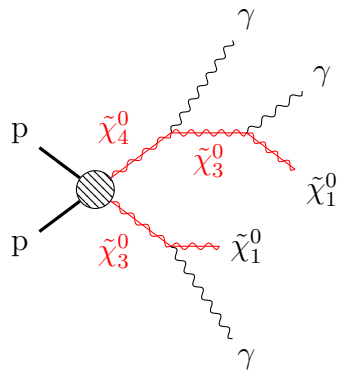

Figure 2.1: Feynman diagram of the benchmark model

The Feynman diagram for the benchmark model is shown in Figure 2.1 [32]. The production cross section of this process (p p > $\tilde{\chi}_4^0$ $\tilde{\chi}_3^0$) is 6.57 fb and the cross section × branching ratio for the three photon and $E_{\mathrm{T}}^{\mathrm{miss}}$ final state is 0.97 fb. The $\tilde{\chi}_1^0$ in this model is almost pure $\tilde{\eta}_1$, the $\tilde{\chi}_3^0$ is almost pure $\tilde{B}^0$ while the $\tilde{\chi}_4^0$ is a mix of the singlino, $\tilde{H}_u$ and $\tilde{H}_d$. See Table 2.6 for more information about the model.

Particle	Mass (GeV)	BR	Components
$\tilde{\chi}_4^0$	447	0.35	$0.69\tilde{S} + 0.16\tilde{H}_u + 0.16\tilde{H}_d$
$\tilde{\chi}_3^0$	292	0.67	$0.97\tilde{B} + 0.015\tilde{H}_u + 0.015\tilde{H}_d$
$\tilde{\chi}_1^0$	4.5	–	$0.99\tilde{\eta}_1 + 0.0026\tilde{\eta}_3 + 0.0026\tilde{\eta}_2$

Table 2.6: Properties of SUSY particles in the benchmark model. The BR in column three is to a lighter neutralino and a photon.

Chapter 3

Experimental work

3.1 Experimental setup

3.1.1 The Large Hadron Collider (LHC)

The Large Hadron Collider (LHC) is a 27 km circumference particle collider at the European Organization for Nuclear Research center (CERN) near Geneva. The LHC has two rings with counter-rotating beams of protons or heavy ions which collide at four detectors; ATLAS [33], CMS [6], ALICE [33] and LHCb [34]. Both ATLAS and CMS are general-purpose detectors, investigating a broad range of physics. These detectors have the same scientific goals, but use different technical solutions and magnet-system design. ALICE studies heavy ion collisions and LHCb studies b-quarks.

The particle beams are guided and accelerated up to an energy of 6.5 TeV by electromagnetic fields, resulting in a centre of mass collision energy of $\sqrt{s} = 13$ TeV. The number of collisions (so-called events) per second that result in a specific process ($R_{\text{proc}}^{\text{events}}$) is given by the luminosity L (which depends on the beam parameters) and the cross section of the process σ_{proc} [35]:

$$R_{\text{proc}} = L\sigma_{\text{proc}} \tag{3.1}$$

The luminosity of the most recent run of LHC is $2.1 \times 10^{34}\text{cm}^2\text{s}^{-1}$. The luminosity can be integrated over time to give the integrated luminosity $\mathcal{L} = \int L dt$. The product of the integrated luminosity and the cross section of a specific process gives the total number of events of that process contained

in the dataset:

$$N_{\text{proc}}^{\text{event}} = \mathcal{L}\sigma_{\text{proc}} \tag{3.2}$$

The integrated luminosity of the LHC Run 2 is 139 fb^{-1}.

3.1.2 The ATLAS detector

ATLAS is a 7000-tonne detector situated in a cavern 100 meters below the ground surface. The detector consists of different subsystems that measure the paths, momenta and energies of the particles that emerge as a result of the collisions. The subdetector closest to the beam line is the inner detector (ID), which measures the tracks of charged particles. The ID is immersed in an axial magnetic field from a solenoid magnet which allows for a measurement of the momenta of charged particles and it consists of the Pixel detector, the Semiconductor tracker and the Transition radiation tracker. The next layer contains two types of calorimeters, the LAr electromagnetic calorimeter to measure the energy of electrons and photons and the Tile calorimeter to measure the energy of hadronic showers. Outside the calorimeters is the muon spectrometer (MS), used to detect muons. Large toroid magnets provide a magnetic field in the MS which allows for a standalone measurement of muon momenta. See Figure 3.1 for an overview of the ATLAS detector.

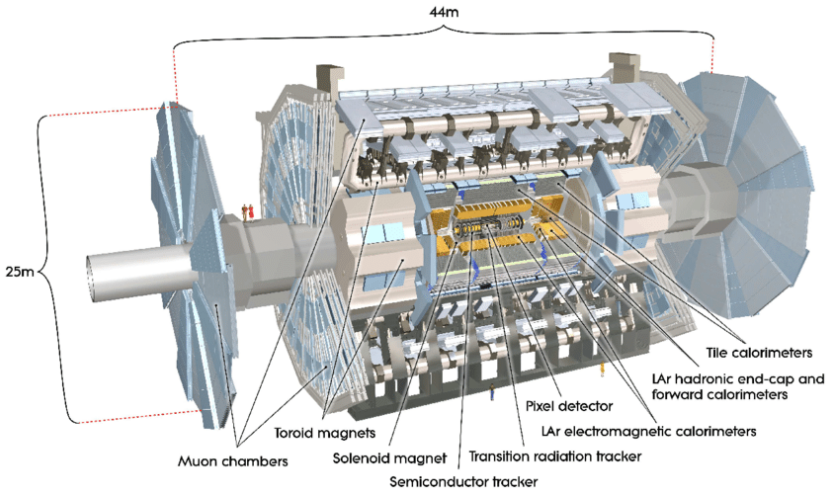

Figure 3.1: Cut-away view of the ATLAS detector

To describe the kinematics of interactions in ATLAS a right-handed coordinate system is used. The z-direction is defined as the direction along the beam line, the direction from the interaction point to the center of the LHC ring is the x-direction and the y-direction is pointing upwards. Usually cylindrical coordinates are used, where ϕ is the azimuthal angle around the beam in the transverse (x-y) plane and the polar angle, θ, the angle away from the beam direction. The polar angle defines the pseudorapidity $\eta = -\ln\tan\frac{\theta}{2}$ which is used for massless objects. For objects with mass rapitidy is used, defined as $y = \frac{1}{2}\ln(\frac{E+p_z}{E-p_z})$. The angular seperation between two particles is given by $\Delta R = \sqrt{(\Delta\eta)^2 + (\Delta\phi)^2}$. Since the momentum in the z-direction before the collision is unknown, transverse quantities like transverse momentum ($\boldsymbol{p}_{\mathrm{T}}$) are generally used. The transverse momenta of charged particles are measured through the curvature of their paths in a strong magnetic field and the calorimeters measure the energies of particles. Since muons do not interact much with matter, they do not stop in the calorimeters, so special muon detectors in the outer layer of the detector measure the muons.

3.1.3 Data acquisition

The detectors in ATLAS have a data output rate of 50 TB per second. This is by far too much data for ATLAS to be able to handle and moreover most of these processes stored in the data are not of interest for researchers. This means that a selection needs to be made to decide which data is interesting. The system responsible for making the first selection is the trigger system, which consists of the L1 and HLT trigger. The L1 trigger is a hardware based trigger that identifies Regions-of-Interest (RoI's) with high transverse-momentum muons, electrons, photons, jets and τ leptons and large momentum imbalance. These RoI's are then fed to the HLT trigger that runs reconstruction software with precision tracking and more sophisticated energy measurements to determine which events are selected.

3.2 Data preparation

3.2.1 Data simulation and reconstruction

In order to estimate ATLAS' sensitivity to various models, simulated data can be used. Simulated data is produced by first defining a model and using that model to generate events in an event generator. During the event generation, most event generators assign a weight to each event that needs to be used in analyses. After that the process of quarks and gluons forming hadrons, called hadronisation, and the showering of particles is calculated by specific software. This results in 4-vectors of particles, containing their energies and momenta, that describe the full event. These are passed onto the detector simulator step in which the toolkit Geant4 [36] is used. Geant4 simulates the passage of particles through the various structures of matter in the detector and outputs the energy that the particles deposit there. Then, in the digitization step, ATLAS software is used to transform the energy deposits into electronic detector read-outs similar to the read-outs obtained from real collisions in the ATLAS detector.

The data that is obtained in this way goes trough ATLAS reconstruction software so that it transforms into a useful data format for data analyses. This reconstruction software identifies particles and their properties and exports that data in so-called xAOD files [37]. The xAOD files contain particle containers in which the particles and their properties for each event are stored. The containers can then easily be accessed with analysis code using Eventloop, a software package that can be used in ROOT [38].

In order to reduce the size of the xAOD files and make them more accessible for analyses, derivations of these files for specific groups or searches are made, so-called DAODs. These derivations are made by selecting events that pass certain criteria, this is called skimming. In this thesis the derivations 'SUSY1' and 'SUSY12' are used. The selection critera for these will be described in Section 3.4.

In this thesis the signal events are analyzed at generator (truth) level. The simulated background events are on the other hand passed through a detector simulation and reconstructed with the ATLAS reconstruction software and are therefore analyzed at so-called reco level.

3.2.2 Particle identification

As described above, the ATLAS reconstruction software identifies particles. The way different particles are identified by this software is described below.

Photons and electrons
Photons and electrons are identified using the electromagnetic calorimeter (EC) and the inner detector (ID). Electrons are seperated from photons by matching the energy deposits in the EC to the tracks measured in the ID; electrons will have a track of a charged particle and photons do not have a matching track. A photon can convert to an $e+e-$ pair in the inner detector, if this happens it is flagged. If the measurement in the EC matches a flagged track, the flagged particle is identified as a photon.

Jets
Jet is a term used to describe a collection of hadrons that come from the showering and hadronization of a quark or gluon. It can be thought of as a cone in the detector in which products of these mentioned processes deposit their energies. The cone size is $\Delta R = \sqrt{(\Delta\eta)^2 + (\Delta\phi)^2}$. The calorimeters measure the jet energy and direction.

Muons
From tracks reconstructed in the muon spectrometers combined with the tracks detected by the ID, muons can be reconstructed.

Missing transverse energy
The missing transverse momentum ($\boldsymbol{E}_{\mathrm{T}}^{\mathrm{miss}}$) of an event is calculated as the negative vector sum of the momenta of all visible particles. This is because the initial transverse energy before the collision is zero, since the colliding particles move along the z-axis and the transverse plane is orthogonal to it. The magnitude of the $\boldsymbol{E}_{\mathrm{T}}^{\mathrm{miss}}$ vector is denoted missing transverse energy ($E_{\mathrm{T}}^{\mathrm{miss}}$). When using simulated data at truth level, the $\boldsymbol{E}_{\mathrm{T}}^{\mathrm{miss}}$ can be calculated as the sum of the momenta of all the invisible particles. Invisible particles are particles that do not interact with the detector, like neutrinos and neutralinos.

Detector inaccuracies or incorrect momentum measurements of visible particles can affect the $\boldsymbol{E}_{\mathrm{T}}^{\mathrm{miss}}$, an effect that would be lacking in the truth-level definition of this quantity.

$H_{\mathbf{T}}$
The total transverse energy H_{T} is defined as the scalar sum of transverse momenta of the visible particles in an event.

3.2.3 Object selection

The simulated background samples used in the background analysis in this thesis have been passed through a simulation of the ATLAS detector and the ATLAS reconstruction software. This process transforms the truth-level data into reconstructed data. It is possible that particles are misidentified in this process. In order to limit background processes from mimicking the signal due to such misidentified particles, certain selection criteria are required of the particles. Only particles that fulfill these criteria are taken into account in the analysis. An overview of the selection criteria that are used in the analysis in this thesis is found in Table 3.1. Objects that pass these selections are in the rest of this thesis referred to as jets, electrons, muons and photons. Details and additional information about the selection criteria in Table 3.1 are listed below. These criteria are in accordance with official ATLAS recommendations and are similar to criteria used in a search with a diphoton and $E_{\mathrm{T}}^{\mathrm{miss}}$ signature in the final state [39].

Objects	Quality	p_{T}-cut	$\lvert\eta\rvert$-cut	Isolation	Other
Jets		30 GeV	2.8		JVT$>$ 0.59 if $p_{\mathrm{T}} < 60$ GeV
Electrons		25 GeV	2.47	"GradientLoose"	excluding $1.37 < \lvert\eta\rvert < 1.52$
Muons	Medium	25 GeV	2.7	"GradientLoose"	
Photons	Tight	25 GeV	2.47	"FixedCutTightCaloOnly"	excluding $1.37 < \lvert\eta\rvert < 1.52$

Table 3.1: Selection criteria for objects used for the analysis in this thesis. Definitions can be found below.

- The quality of electrons, muons and photons can be classified as either 'loose', 'medium' or 'tight'. The classification of electrons and photons is based on variables describing the shape of the electromagnetic shower

in the calorimeters, with the electron classification making use of additional requirements on e.g. the quality of the associated track, the track matching and the energy-to-momentum ratio. See Refs. [40, 41] for details and definitions regarding the quality of photons and Refs. [42, 43, 44] for electrons.
The classification of muons is based on the number of hits in the inner detector and muon spectrometers as well as on the significance of the charge-to-momentum ratio. See Ref. [45] for additional information.

- The isolation of an object can be either 'loose', 'medium' or 'tight'. This label judges how isolated one object is with respect to other objects. The requirement for this label can either depend on the mass or energy of the object ('gradient') or not depend on the properties of the object at all ('fixed cut'). The label 'FixedCutTightCaloOnly' means for example that a the cut on the isolation of the particle is based on calorimeter measurements only and does not depend on the properties of the object.

- The region $1.37 < |\eta| < 1.52$ is excluded because this is a transition region in the calorimeter, causing measurements in this region to be unreliable.

- JVT stands for jet-vertex-tagger. This is an algorithm that rejects jets that do not come from the hard scatter processes, but instead emerge from separate proton-proton collisions in the same bunch-crossing as the signal. These are called pileup jets. To identify pileup jets, the JVT algorithm makes use of the tracks associated to the jet and counts the fraction of tracks that originate from the hard-scatter vertex and from vertices from pileup interactions. See ref. [46] for more detailed information.

3.2.4 Overlap removal

When the data goes through the reconstruction process, it is possible that multiple objects are reconstructed from the same detector signal. This means that one object could be stored in two different particle containers in the DAOD files. In order to prevent double counting, a so-called overlap removal needs to be carried out before analyzing the data. This overlap removal is based on the ΔR of two objects, describing how much the objects as

measured in the detectors are separated from each other. For example if particle A defines the reference direction, then $\Delta R(\mathrm{A}, \mathrm{B}) < 0.4$ means that particle B is within a cone of radius 0.4 around particle A. If two different objects overlap too much, one of the objects is removed and not used further in the analysis. The steps of the overlap removal are described below.

1. If $\Delta R(\text{jet}, \text{electron}) < 0.2$: the jet is removed
2. If $0.2 < \Delta R(\text{electron}, \text{jet}) < 0.4$: the electron is removed
3. If $\Delta R(\text{muon}, \text{jet}) < 0.4$: the muon is removed
4. If $\Delta R(\text{photon}, \text{electron}) < 0.4$: the photon is removed
5. If $\Delta R(\text{photon}, \text{muon}) < 0.4$: the photon is removed
6. If $\Delta R(\text{jet}, \text{photon}) < 0.4$: the jet is removed

3.3 Simulated signal samples

In order to study the properties of events generated by the benchmark model in this thesis and compare it to possible background events, a sample of simulated data for the signal benchmark model needs to be made. The first step of making this signal sample is to create a model and run that through an event generator. The benchmark model studied in this thesis is made in FeynRules [47], a Mathematica package that can calculate the Feynman rules for any model. When the full Lagrangian, mixing angles, coupling parameters and other free parameters are given to FeynRules, the software can calculate the Feynman rules of the model and outputs these in a so-called UFO-file. This UFO-file is passed onto the next-to-leading order matrix element generator MadGraph5 [48], which uses Monte Carlo (MC) based algorithms to generate the hard-scatter processes. After that the hadronisation and showering of particles is calculated at lowest order by Pythia [49, 50]. After these steps only 4-vectors of particles containing their energies and momenta are left to describe the events in the sample. MadAnalysis [51] is used to analyze these.

3.4 Simulated background samples

When looking for physics Beyond the Standard Model (BSM), it is necessary to estimate the expected contribution from background processes. In this case background processes are Standard Model processes that result in the same detector signature as the BSM process sought for. This could be caused either by the signal and background processes having the same final state particles or by measurement inaccuracies causing a background process with different final state particles than the signal showing up in data as having the same final state particles as the signal. In this thesis simulated data samples prepared as described in Section 3.2 are used to analyze the background processes. These samples are produced and made available by the ATLAS collaboration.

The signature with three photons and $E_{\mathrm{T}}^{\mathrm{miss}}$ in the final state as described in Section 2.3 is only extremely rarely produced by the Standard Model. There are however SM processes that can give the same signature in data as this process due to measurement inaccuracies. Six groups of SM production processes have been analyzed in this thesis. Table 3.2 shows an overview of these background groups.

Group	Background	Fake photons	Fake $E_{\mathrm{T}}^{\mathrm{miss}}$	MC sample numbers
γj	$\gamma + jet$	2	yes	361039 - 361062
$Z\gamma$	$Z \to \ell\ell + jets + \gamma$	2	yes	364500 - 364514
	$Z \to \nu\nu + jets + \gamma$	2	no	364517 - 364519
$W\gamma$	$W \to \ell\nu + jets + \gamma$	2	no	364521 - 364535
$W\gamma\gamma$	$W \to \ell\nu + \gamma\gamma$	1	no	407022 - 407024
$Z\gamma\gamma$	$Z \to \ell\ell + \gamma\gamma$	1	yes	407025 - 407027
	$Z \to \nu\nu + \gamma\gamma$	1	no	407028
$\gamma\gamma\gamma$	$\gamma\gamma\gamma$	0	yes	407318

Table 3.2: Analyzed backgrounds for the three photon and $E_{\mathrm{T}}^{\mathrm{miss}}$ signature and the detector inaccuracies required in order to have similar signatures as the signal.

The first group corresponds to SM processes that produce two photons or one photon and a jet, referred to as γj. However, only samples with one photon and a jet have been analyzed in this thesis since the two photon samples were unavailable. In order for this process to produce the same signature as the signal, two so-called fake photons need to be present. A fake photon is a non-photonic particle that is misidentified as a photon in the reconstruction and identification process (see Sections 3.2.1 and 3.2.2). The events also need to have a large amount of fake $E_{\mathrm{T}}^{\mathrm{miss}}$.

The second and third group consist of processes that produce a Z or W boson, one photon and at least one jet, referred to as $Z\gamma$ and $W\gamma$. In order for these processes to give the same signature as the signal, two so-called fake photons need to be present in data. Additionally if the Z or W boson does not decay to neutrinos, fake $E_{\mathrm{T}}^{\mathrm{miss}}$ is needed.

The fourth and fifth groups of background processes are those in which a W or Z boson is produced together with two photons, referred to as $W\gamma\gamma$ and $Z\gamma\gamma$. For these to have the same signature as the signal, one fake photon and, for some decay modes, fake $E_{\mathrm{T}}^{\mathrm{miss}}$ is needed.

The last group consists of SM processes in which three final state photons are produced, referred to as $\gamma\gamma\gamma$. For this process to have the same signature as the signal, only fake $E_{\mathrm{T}}^{\mathrm{miss}}$ is needed.

The simulated background samples used in this thesis are SUSY1 and SUSY12 derivations of xAOD files (see Table 3.3). The SUSY1 derivation is preferred, however for some samples this derivation was not available and the derivation SUSY12 is used instead. The SUSY12 derivation has a harder cut on the leading photon p_{T} and requires a jet. This is not optimal and could have some impact on the final result. The effect is however expected to be small since the SUSY1 derivations are used for the dominant background processes.

	event selection
SUSY1	$H_{\mathrm{T}} > 150$ GeV **OR** e, μ $\mathrm{p_T} > 100$ GeV **OR** photon $\mathrm{p_T} > 100$ GeV **OR** $2e/\mu$ $\mathrm{p_T} > 20$GeV **OR** 2 photons $p_{\mathrm{T}} > 50$GeV
SUSY12	$E_{\mathrm{T}}^{\mathrm{miss}}$ **AND** 1 jet/e $\mathrm{p_T} > 150$ GeV **OR** ($E_{\mathrm{T}}^{\mathrm{miss}}$ **OR** e **OR** μ) **AND** e/μ $\mathrm{p_T} > 20$ GeV **AND** 1 jet $\mathrm{p_T} > 80$ GeV **OR** photon $\mathrm{p_T} > 100$ GeV **AND** 1 jet > 80 GeV

Table 3.3: Selection criteria of the SUSY1 and SUSY12 DAODs. For the definition of H_{T}, see 3.2.2

A complete list of the samples used in this thesis can be found in Appendix D. The name of the datasample desribes which derivation is used for that specific sample. Table 3.4 shows the impact of the skimming, which is imposed in the derivation step, on the various background groups.

Background	Total weight before skimming	Total weight after skimming	Total number of events after skimming
γj	63195766.0	23529095.8	23415532
$Z\gamma$	22233797.9	6943077.8	9742800
$W\gamma$	68128550.4	2109706.2	2628579
$W\gamma\gamma$	30263.6	18603.8	18508
$Z\gamma\gamma$	39124.8	25440.4	25355
$\gamma\gamma\gamma$	99998.0	2662.0	2662
Total	153727500.8	32628586.0	35833436

Table 3.4: The sum of event weights and the total number of events per background group before and after the skimming performed in the derivation step.

3.5 Background estimate

In order to test the presence of BSM physics, the measured number of events in the detector is compared to the predictions made by the SM. If there are significantly more events with the signature in the data than predicted by the SM, it could point towards BSM physics. Before using real data to test the

presence of BSM physics, simulated data can be used to determine if one expects a particular BSM model to generate a significant excess of data events with a particular signature compared to the number of expected events from the SM alone.

In this thesis the simulated background samples are used to determine the number of expected events with a three photon and $E_{\mathrm{T}}^{\mathrm{miss}}$ signature from SM processes. The expected number of background events passing a given selection, $N_{\mathrm{bkg}}^{\mathrm{exp}}$, is calculated with the following formula

$$N_{\mathrm{bkg}}^{\mathrm{exp}} = \mathcal{L} \times \sigma \times \epsilon_{\mathrm{filter}} \times \frac{\sum_{i \in \mathrm{sel}} w_i}{\sum_{i \in \mathrm{all}} w_i} \tag{3.3}$$

where $\mathcal{L}$ is the integrated luminosity, chosen to be 139 fb^{-1} which corresponds to the integrated luminosity of the ATLAS Run-2 dataset, $\sigma \times \epsilon_{\mathrm{filter}}$ is the cross section of the simulated process in fb, $\sum_{i \in \mathrm{sel}} w_i$ is the sum of the event weights of the events passing the selection and $\sum_{i \in \mathrm{all}} w_i$ is the summed event weight in the sample before skimming.

There are multiple skimming criteria applied when producing the DAODs (see Section 3.4) that have been applied to the background samples but not the signal samples. Thus a preselection of the events is made requiring an event to have at least one photon with $p_{\mathrm{T}} > 100$ GeV and at least two photons with $p_{\mathrm{T}} > 50$ GeV. The resulting sample is referred to as the preselected background sample. Table 3.5 shows the raw event counts and the number of expected events, derived using Equation 3.3 for the various backgrounds in the preselected sample.

Background	Event counts in preselection	Expected events in preselection
γj	18907 ± 138	40052 ± 1534
$Z\gamma$	4865 ± 70	324 ± 17
$W\gamma$	3632 ± 60	721 ± 33
$W\gamma\gamma$	3656 ± 60	1328 ± 22
$Z\gamma\gamma$	4504 ± 67	221 ± 3
$\gamma\gamma\gamma$	556 ± 24	241 ± 10
Total background	$\mathbf{36120 \pm 190}$	$\mathbf{42887 \pm 1535}$

Table 3.5: The event counts and expected number of events in the preselected sample for a luminosity of 139 fb^{-1}.

Figure 3.2 shows the p_{T} distribution of the leading, second leading and third leading photons in the preselected background sample. Since the events in these backgrounds often lack a third or even second photon, the histograms have been scaled to unit area to make the second and third photon p_{T} distributions more visible. The $E_{\mathrm{T}}^{\mathrm{miss}}$ distribution is displayed in Figure 3.3, where the histogram has been scaled to the expected number of background events. Some events can have a negative event weight, which explains the negative number of events around 280 GeV. Figure 3.4 shows the distribution of $\Delta\phi_{\mathrm{min}}(\gamma, \boldsymbol{E}_{\mathrm{T}}^{\mathrm{miss}})$. $\Delta\phi_{\mathrm{min}}(\gamma, \boldsymbol{E}_{\mathrm{T}}^{\mathrm{miss}})$ is the minimum absolute difference in ϕ between the $\boldsymbol{E}_{\mathrm{T}}^{\mathrm{miss}}$ and each of the photons 4-vectors. A cut on $\Delta\phi_{\mathrm{min}}(\gamma, \boldsymbol{E}_{\mathrm{T}}^{\mathrm{miss}})$ could reduce the amount of fake $E_{\mathrm{T}}^{\mathrm{miss}}$.

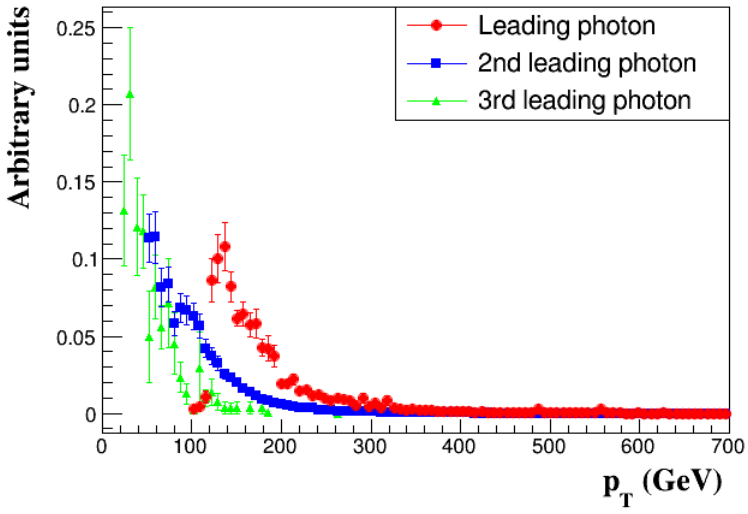

Figure 3.2: Photon p_{T} distribution scaled to unit area in the preselected background sample. The red line shows the distribution of the leading photons, the blue of the second leading photon and the green of the third leading photon.

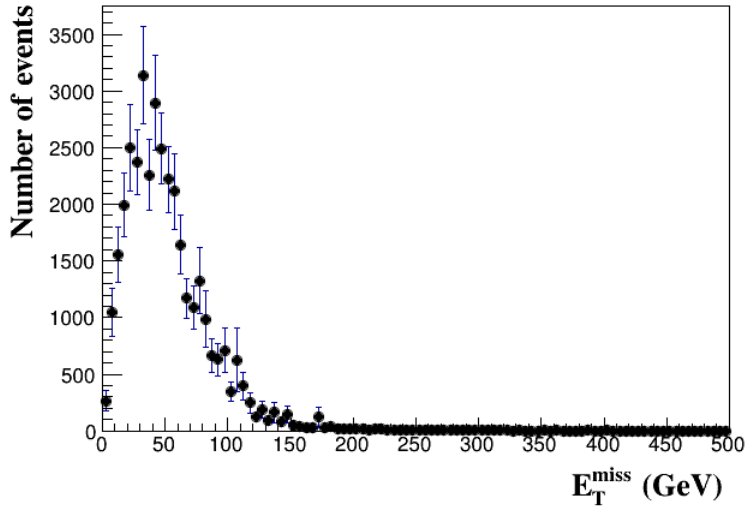

Figure 3.3: $E_{\mathrm{T}}^{\mathrm{miss}}$ distribution, scaled to the total number of events in the preselected background sample.

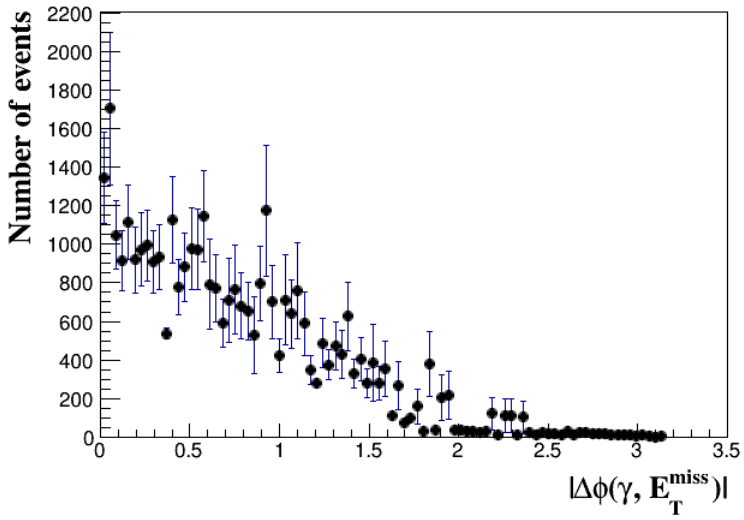

Figure 3.4: $\Delta\phi_{\min}(\gamma, \boldsymbol{E}_{\mathrm{T}}^{\mathrm{miss}})$ distribution scaled to the toal number of events in the the preselected background sample.

3.6 Signal estimate

The signal sample is made by generating 10000 events as described in Section 3.3, resulting in the signal data sample that contains truth-level information about the benchmark model described in Section 2.3.3. Since this signal sample will be compared to the background sample, the same p_{T} and $|\eta|$ cuts are imposed on the photons, see Table 3.1. After these cuts are imposed, the same preselection as for the preselected background sample is made for the signal sample, resulting in what is referred to as the preselected signal sample. Since the events in the signal sample all have the same weights, the expected number of selected signal, $N_{\mathrm{sig}}^{\mathrm{exp}}$ is calculated with the following formula:

$$N_{\mathrm{sig}}^{\mathrm{exp}} = \mathcal{L} \times \sigma \times \frac{N_{\mathrm{sel}}}{N_{\mathrm{all}}} \tag{3.4}$$

where $\mathcal{L}$ is the integrated luminosity of 139 fb^{-1}, σ the cross section of the signal sample, $\sigma = 0.97$ fb^{-1}, N_{sel} and N_{all} the number of selected events and the total number of events in the sample, respectively. 9082 out of 10000 events pass the preselection cuts, leading to an expectation of 122.1 signal events in the preselected sample.

Since the events in the preselected signal sample are analyzed at truth level, the $E_{\mathrm{T}}^{\mathrm{miss}}$ is calculated as the sum of the p_{T}'s of the two final state neutralinos. These neutralinos would in an experiment not interact with the detector and thus be measured as $E_{\mathrm{T}}^{\mathrm{miss}}$. Any detector uncertainties or other sources of $E_{\mathrm{T}}^{\mathrm{miss}}$ are not taken into account in this calculation of the $E_{\mathrm{T}}^{\mathrm{miss}}$.

Figure 3.5 shows the p_{T} distribution of the leading, second leading and third leading signal photons, Figure 3.6 shows the $E_{\mathrm{T}}^{\mathrm{miss}}$ distribution and Figure 3.7 shows the distribution of $\Delta\phi_{\mathrm{min}}(\gamma, \boldsymbol{E}_{\mathrm{T}}^{\mathrm{miss}})$ in the preselected signal sample.

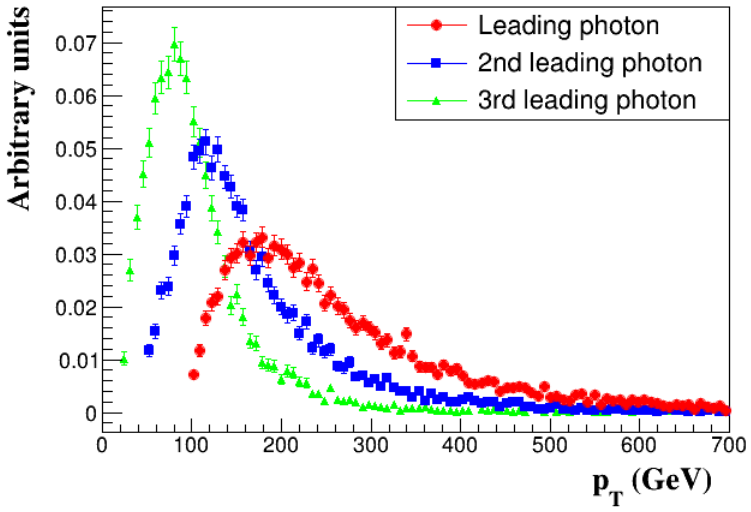

Figure 3.5: p_{T} distribution of the signal photons at truth level, scaled to unit area. The red line shows the distribution of the leading photon, the blue of the second leading photon and the green of the third leading photon.

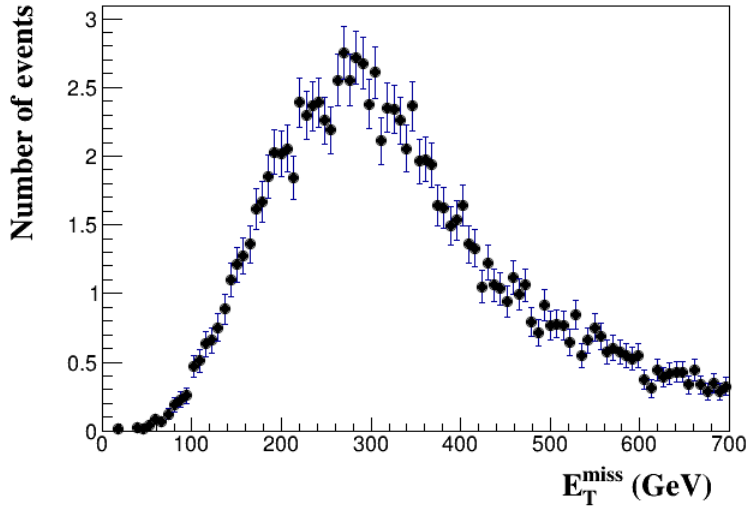

Figure 3.6: Distribution of the $E_{\mathrm{T}}^{\mathrm{miss}}$ of the signal scaled to the expected number of events in the preselected signal sample. The $E_{\mathrm{T}}^{\mathrm{miss}}$ is defined as the sum of the p_{T}'s of the two final state neutralinos.

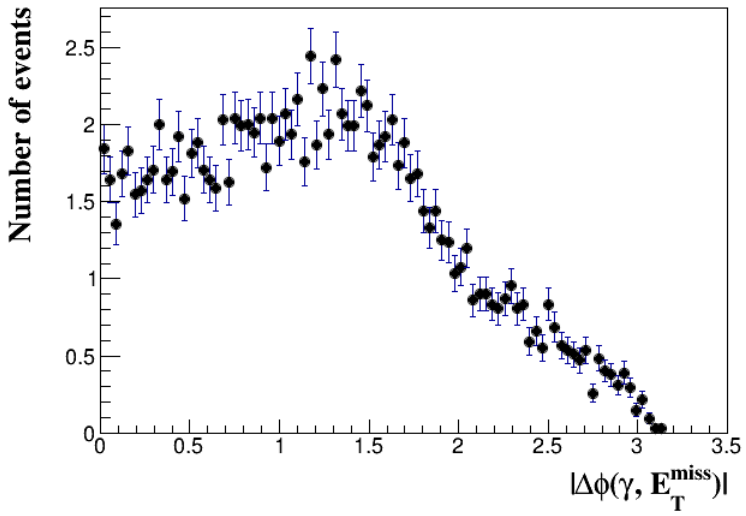

Figure 3.7: $\Delta\phi_{\mathrm{min}}(\gamma, \boldsymbol{E}_{\mathrm{T}}^{\mathrm{miss}})$ distribution of the preselected signal sample scaled to the expected number of events in the preselected signal sample.

3.7 Three-photon signal region optimization

With the procedure established for how to estimate the expected number of background and signal events, it can be determined if the benchmark model would yield a significant increase the number of data events passing a given selection. To determine this, the discovery significance Z is calculated with the following formula [52]:

$$Z = \sqrt{2(n \ln[\frac{n(b+\sigma^2)}{b^2+n\sigma^2}] - \frac{b^2}{\sigma^2}\ln[1+\frac{\sigma^2(n-b)}{b(b+\sigma^2)}])} \tag{3.5}$$

where s is the number of signal events, b the number of background events, $n = s+b$ and σ the systematic uncertainty on the background estimate, here assumed to be $\sigma = 0.2 \times b$. A Z above 5 would allow for a discovery.

In the preselected sample $b = 42887 \pm 1535$ and $s = 122.1 \pm 1.3$ making $Z = 0.01$. This means that no significant excess over the SM background is expected in the preselected sample, even for the case when the benchmark model is realized in data. The discovery significance can however be improved by imposing cuts on certain quantities. Comparing the photon p_{T} distribution of the preselected backround and signal samples (Figures 3.2 and 3.5) makes clear that the signal photons have higher p_{T} than the ones in the background. Additionally, looking at Figures 3.3 and 3.6, the $E_{\mathrm{T}}^{\mathrm{miss}}$ of the signal events is on average higher than that of the background events and the same is true for $\Delta\phi_{\mathrm{min}}(\gamma, \boldsymbol{E}_{\mathrm{T}}^{\mathrm{miss}})$ (see Figures 3.4 and 3.7). This means that cuts imposed on these quantities could reduce the amount of background events, while keeping a relatively big part of the signal events.

In order to choose the optimal set of cuts, the Z significance is determined as a function of cut values on leading, second leading and third leading photon p_{T}, $E_{\mathrm{T}}^{\mathrm{miss}}$ and $\Delta\phi_{\mathrm{min}}(\gamma, \boldsymbol{E}_{\mathrm{T}}^{\mathrm{miss}})$. In each step the cut corresponding to the maximal Z is chosen and implemented before determining the optimal value for the next cut. First the Z significance is calculated as a function of cut value on the third leading photon p_{T}, see Figure 3.8.

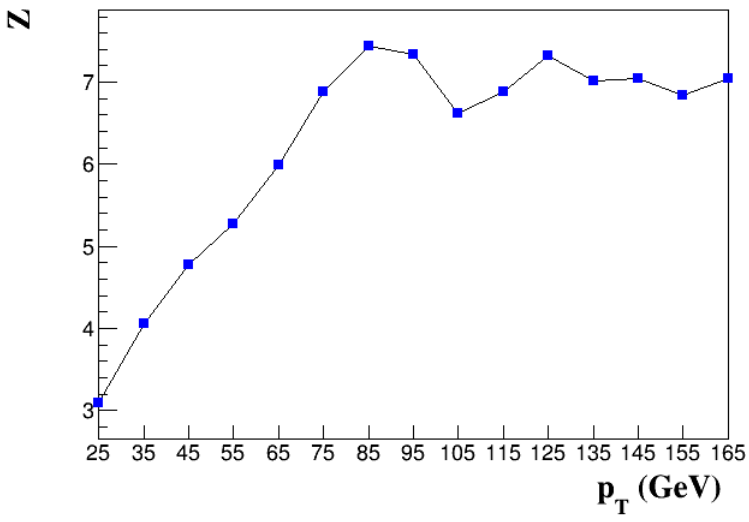

Figure 3.8: Z significance as a funtion of the cut value on p_{T} of the third leading photon.

Above a p_{T} cut of 85 GeV on the third leading photon the Z significance flattens, so this is implemented as the first cut value. Thereafter the same is done for the second leading photon p_{T}, see Figure 3.9. The Z significance as a function of second leading photon p_{T} flattens above a cut value of 105 GeV. This value is implemented as a cut value and the Z significance as a function of leading photon p_{T} cuts is calculated next, see Figure 3.10. The Z significance does not increase for cut values on the leading photon p_{T} higher than 105 GeV and thus this value is implemented as cut value. The next quantity on which a cut can be placed is $E_{\mathrm{T}}^{\mathrm{miss}}$. Figure 3.11 shows that the Z significance increases until a $E_{\mathrm{T}}^{\mathrm{miss}}$ cut of 80 GeV, after which it starts decreasing. Consequently 80 GeV is chosen as a cut value on the $E_{\mathrm{T}}^{\mathrm{miss}}$. Lastly, the Z significance is calculated as a function of $\Delta\phi_{\mathrm{min}}(\gamma, \boldsymbol{E}_{\mathrm{T}}^{\mathrm{miss}})$ cuts, see Figure 3.12. As visible in Figure 3.9 the Z significance strictly decreases as the $\Delta\phi_{\mathrm{min}}(\gamma, \boldsymbol{E}_{\mathrm{T}}^{\mathrm{miss}})$ cuts becomes stricter, thus there is no cut implemented on $\Delta\phi_{\mathrm{min}}(\gamma, \boldsymbol{E}_{\mathrm{T}}^{\mathrm{miss}})$ (i.e. $\Delta\phi_{\mathrm{min}}(\gamma, \boldsymbol{E}_{\mathrm{T}}^{\mathrm{miss}}) > 0$).

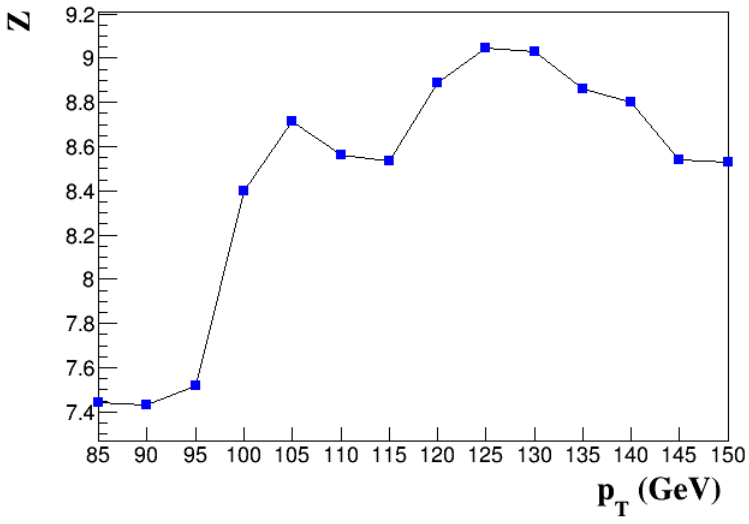

Figure 3.9: Z significance as a funtion of the cut value on the p_{T} of the second leading photon.

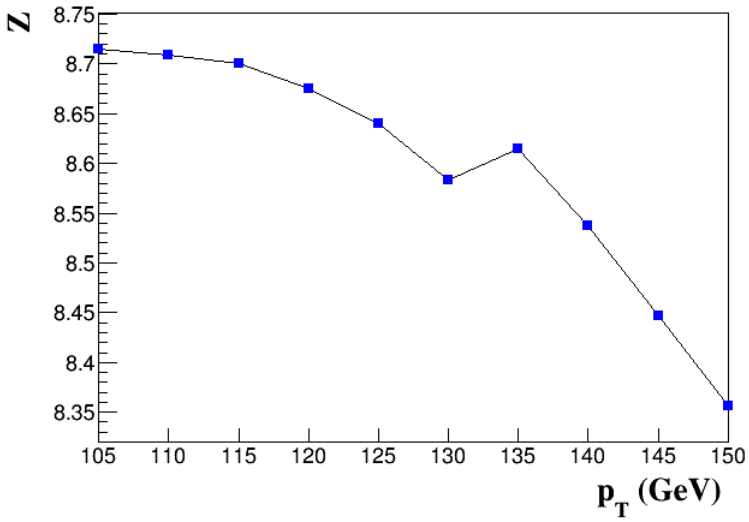

Figure 3.10: Z significance as a funtion of the cut value on the p_{T} of the leading photon.

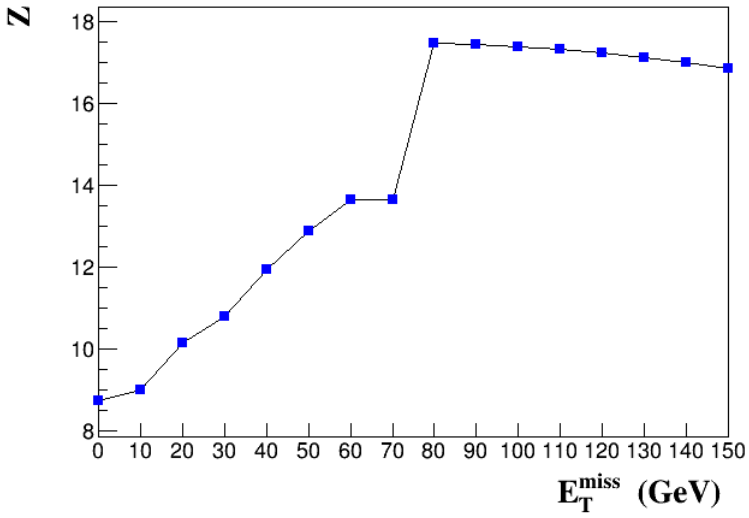

Figure 3.11: Z significance as a funtion of cut value on $E_{\mathrm{T}}^{\mathrm{miss}}$.

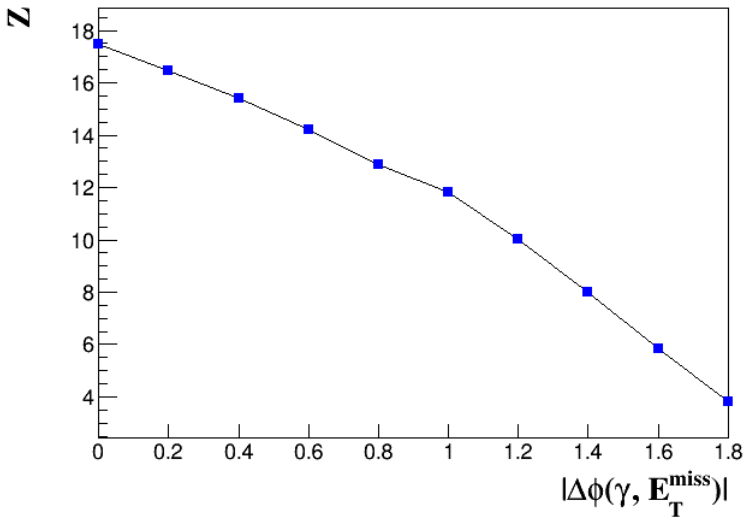

Figure 3.12: Z significance as a funtion of cut value on $\Delta\phi_{\mathrm{min}}(\gamma, \boldsymbol{E}_{\mathrm{T}}^{\mathrm{miss}})$.

The process of optimizing the Z significance as described above results in the following cut values:

- Third leading photon (γ_3) $p_{\mathrm{T}} > 85$ GeV
- Second leading photon (γ_2) $p_{\mathrm{T}} > 105$ GeV
- Leading photon (γ_1) $p_{\mathrm{T}} > 105$ GeV
- $E_{\mathrm{T}}^{\mathrm{miss}} > 80$ GeV

This set of selection critera are referred to as the Signal Region (SR). The Z significance at each step in this cutflow is summarized in Table 3.6.

Cut	s	b	Z	event count signal	event count background
Preselection	122.1 ± 1.3	42887.5 ± 1534.8	0.01	9082 ± 95	36120 ± 190
γ_3 $p_{\mathrm{T}} > 85$ GeV	52.0 ± 0.8	12.6 ± 3.3	7.4	3866 ± 62	33 ± 6
γ_2 $p_{\mathrm{T}} > 105$ GeV	50.0 ± 0.8	8.1 ± 1.8	8.7	3717 ± 61	26 ± 5
γ_1 $p_{\mathrm{T}} > 105$ GeV	50.0 ± 0.8	8.1 ± 1.8	8.7	3717 ± 61	26 ± 5
$E_{\mathrm{T}}^{\mathrm{miss}} > 80$ GeV	49.7 ± 0.8	0.5 ± 0.4	17.5	3701 ± 61	3 ± 2
$\Delta\phi_{\mathrm{min}}(\gamma, \boldsymbol{E}_{\mathrm{T}}^{\mathrm{miss}}) > 0$	49.7 ± 0.8	0.5 ± 0.4	17.5	3701 ± 61	3 ± 2

Table 3.6: The discovery significance Z at each step of the cutflow, the number of expected events for the signal (s) and background (b) and event counts in the SR of the signal and background.

A summary of the expected number of signal and background events in the SR is given in Table 3.7, as well as the event counts in the SR per background. More detailed information about the event count per selection criterion per background can be found in Appendix C. As can be noted, the number of background events passing the SR selection criteria is very small, resulting in a large statistical uncertainty on the expected number of background events and the expected discovery significance.

Background	Event counts after skimming	Event counts in the SR	Expected number of events in the SR
γj	23415532 ± 4839	0	0
$Z\gamma$	8968593 ± 2995	1 ± 1	0.01 ± 0.01
$W\gamma$	2241409 ± 1497	1 ± 1	0.1 ± 0.1
$W\gamma\gamma$	18508 ± 136	1 ± 1	0.4 ± 0.4
$Z\gamma\gamma$	25355 ± 159	0	0
$\gamma\gamma\gamma$	2662 ± 52	0	0
Total background	**35833436 ± 5986**	**3 ± 2**	**0.5 ± 0.4**
Signal	**10000 ± 100**	**3701 ± 61**	**49.7 ± 0.8**

Table 3.7: The event counts after skimming, the event counts in the SR and the expected number of events in the SR for a luminosity of 139 fb^{-1}.

3.8 Model sensitivity in existing search

In Ref. [39] a search is presented for a model with a two photon and $E_{\mathrm{T}}^{\mathrm{miss}}$ signature, referred to as the diphoton search. To see if that search would have found the model presented in this thesis, the expected number of events from the benchmark model passing the selection criteria of each of the four SRs in the diphoton search is estimated. The four signal regions, $\mathrm{SR}^{\gamma\gamma}_{\text{S-L}}$, $\mathrm{SR}^{\gamma\gamma}_{\text{S-H}}$, $\mathrm{SR}^{\gamma\gamma}_{\text{W-L}}$ and $\mathrm{SR}^{\gamma\gamma}_{\text{W-H}}$, are defined in Table 3.8.

Signal region	$\mathrm{SR}^{\gamma\gamma}_{\text{S-L}}$	$\mathrm{SR}^{\gamma\gamma}_{\text{S-H}}$	$\mathrm{SR}^{\gamma\gamma}_{\text{W-L}}$	$\mathrm{SR}^{\gamma\gamma}_{\text{W-H}}$
Number of photons	≥ 2	≥ 2	≥ 2	≥ 2
photon p_{T} (GeV)	> 75	> 75	> 75	> 75
$E_{\mathrm{T}}^{\mathrm{miss}}$ (GeV)	> 150	> 250	> 150	> 250
H_{T} (GeV)	> 2750	> 2000	> 1500	> 1000
$\Delta\phi_{\mathrm{min}}(\mathrm{jet}, \boldsymbol{E}_{\mathrm{T}}^{\mathrm{miss}})$	> 0.5	> 0.5	> 0.5	> 0.5
$\Delta\phi_{\mathrm{min}}(\gamma, \boldsymbol{E}_{\mathrm{T}}^{\mathrm{miss}})$	-	> 0.5	-	> 0.5

Table 3.8: The requirements defining the SRs for the diphoton search.

Since the benchmark model does not contain jets, the requirements on $\Delta\phi_{\min}(\text{jet}, \boldsymbol{E}_{\text{T}}^{\text{miss}})$ are omitted. Table 3.9 shows the number of expected background events estimated in Ref. [39], the number of expected signal events and the Z significance calculated with Equation 3.5 for each SR.

Signal region	Expected background events	Expected signal events	Z
$\text{SR}^{\gamma\gamma}_{\text{S-L}}$	$1.9^{+1.2}_{-1.0}$	0.07 ± 0.03	0.05
$\text{SR}^{\gamma\gamma}_{\text{S-H}}$	$1.8^{+1.2}_{-1.0}$	0.11 ± 0.04	0.08
$\text{SR}^{\gamma\gamma}_{\text{W-L}}$	14.2 ± 4.2	1.6 ± 0.1	0.3
$\text{SR}^{\gamma\gamma}_{\text{W-H}}$	$7.9^{+2.5}_{-2.4}$	3.1 ± 0.2	0.9

Table 3.9: The expected number of background and signal events for the diphoton SRs as well as the Z significance for a luminosity of 139 fb^{-1}.

Since the Z significance of the benchmark model is lower than 5, the analysis carried out in the diphoton search would not have discovered the benchmark model in this thesis with significant certainty if it is realized in nature. The cut removing most of the signal is the cut on H_{T}. So possibly a diphoton search with a looser H_{T} cut could be more sensitive for the benchmark model.

Signal region $\text{SR}^{\gamma\gamma}_{\text{W-H}}$ gives the largest Z significance for the benchmark model. Comparing that to the Z significance obtained by the search strategy proposed in this thesis (see Section 3.7) of 17.5, it seems that the search strategy proposed in this thesis is more suitable to find the benchmark model if it would be realized in nature. However, the poor statistics of the background estimation in this thesis would need to be improved to make a more conclusive comparison. Furthermore, techniques to estimate the background in data rather than simulated events should be used to obtain a more reliable background estimate.

Chapter 4

Conclusions and outlook

4.1 Conclusions

In this thesis, a Next-to-minimal Supersymmetric Model, with gauge mediated SUSY breaking in three hidden sectors, is introduced and the additional particle content and its characteristics are described. As a consequence of SUSY breaking in three hidden sectors, three additional neutralinos are present in the model. Parameters of this model that can give a three photon and $E_{\mathrm{T}}^{\mathrm{miss}}$ final state are found and used to define a signal benchmark model. If this benchmark is realized in nature, it would lead to events with three photons and $E_{\mathrm{T}}^{\mathrm{miss}}$ to be produced at the Large Hadron Collider, and it could thus be searched for with the ATLAS detector.

Using simulated data samples provided by the ATLAS Collaboration, the background for the three photon and $E_{\mathrm{T}}^{\mathrm{miss}}$ signal of the benchmark model is estimated. This is compared to the estimate for the signal and an optimal set of selection criteria is determined, referred to as the signal region. With the expected number of signal and background events in the signal region the discovery significance is calculated to be 17.5. This number however has large uncertainties, due to the limited number of events in the simulated background samples.

Additionally, the sensitivity to this model of a diphoton and $E_{\mathrm{T}}^{\mathrm{miss}}$ search is determined. From this it can be concluded that the discovery significance of the benchmark model with the search strategy from the diphoton paper at

a luminosity of 139 fb^{-1} would be 0.9. This indicates that the search strategy presented in this thesis would be more succesful in finding the benchmark model than the stategy of the diphoton search, if the model exists in nature.

4.2 Outlook

In this thesis, the estimate of the expected number of background events is done with events simulated and reconstructed with software from the ATLAS experiment while the expected number of signal events is estimated at generator-level, without accounting for detector or reconstruction effects. In the future, the signal model could be incorporated into an ATLAS analysis, which could involve passing the signal sample through the ATLAS simulation and reconstruction and carrying out the full analysis at reconstruction level.

Another limitation of the analysis presented in this thesis is the large uncertainty of the background estimate. Not only is the statistical uncertainty of the estimate large because of insufficient statistics in the simulated samples, but also the technique used to estimate the background has clear shortcomings. As discussed in Section 3.4, the main SM background sources contain fake photons or fake $E_{\text{T}}^{\text{miss}}$. Generally such fake backgrounds, which arise from limitations in the detector performance and data reconstruction procedure, are not well modelled by the detector simulation. Instead, techniques that make use of real data are often used to estimate these backgrounds. In order to make the background estimates more reliable, they should be estimated using a combination of simulated and real data, along the lines of what has been done in the diphoton search [39].

Finally, the systematic uncertainty on the background estimate was assumed to be 20% in this thesis. In a future analysis, this number should be properly estimated using the tools and procedures used in other analyses within the ATLAS Collaboration. Based on the findings of the diphoton search, the dominant sources of systematic uncertainty are expected to come from uncertainties in the photon identification and the energy measurements in the calorimeters.

Appendix A

Mixing terms in mass matrix

In order for the integrals to be renormalizable they can have a dimension of maximally 4. Any combination of the following superfields can be integrated as described in equations (2.12), (2.13) and (2.14) to see which terms contribute to the components in the mass matrix. For the mixing matrix $\mathcal{M}_{\tilde{\chi}^0}$ the superfields $\mathbf{H}_u, \mathbf{H}_d, \mathbf{S}, \mathbf{X}_i$ and $\mathbf{W}_\alpha$ are relevant. $\mathbf{H}_u, \mathbf{H}_d$ and $\mathbf{S}$ are chiral superfields of the Higgs and gauge singlet, $\mathbf{X}_i$ with $i = 1, 2, 3$ are the spurion superfields introduced by gauge mediated SUSY breaking and $\mathbf{W}_\alpha$ is the superfield of the gauge supermultiplets. The superfields $\mathbf{H}_u, \mathbf{H}_d, \mathbf{S}, \mathbf{X}_i$ are all chiral superfield and thus have dimension 1, $\mathbf{W}_\alpha$ is a vector superfield with dimension $\frac{3}{2}$ in the Wess-Zumino gauge. The integration factor $d^2\theta$ also has a dimension of one. So without gauge mediation the following integrals have dimension 4:

$$\int d^2\theta \; \phi^3 \tag{A.1}$$

$$\int d^2\theta d^2\theta^\dagger \; \phi^\dagger \phi \tag{A.2}$$

$$\int d^2\theta \; \mathbf{WW} \tag{A.3}$$

where $\phi = \mathbf{H}_u, \mathbf{H}_d, \mathbf{S}$ the chiral superfields.

When gauge mediation is added to the theory one can add one or multiple spurion superfields $\mathbf{X}$ to an integral from eq. (A.1), (A.2) or (A.3), but to keep a dimension of maximally 4, the SUSY breaking scale f_i of that breaking sector must be added as a factor in front. The Spurion superfield is described

by

$$\mathbf{X} = \sqrt{2}\theta\tilde{\eta} + \theta^2 F \tag{A.4}$$

with $\langle F_i \rangle = f_i$. The other relevant superfields look as follows:

$$\mathbf{H}_u = H_u + \sqrt{2}\tilde{H}_u\theta + F_{H_u}\theta^2 \tag{A.5}$$

$$\mathbf{H}_d = H_d + \sqrt{2}\tilde{H}_d\theta + F_{H_d}\theta^2 \tag{A.6}$$

$$\mathbf{S} = S + \sqrt{2}\tilde{S}\theta + F_S\theta^2 \tag{A.7}$$

$$\mathbf{W}_\alpha = \tilde{B}_\alpha + D\theta_\alpha + (\frac{i}{2}\sigma^\mu\bar{\sigma}^\nu\theta)_\alpha B_{\mu\nu} + i\theta^2(\sigma^\mu\partial_\mu\tilde{B}^\dagger)_\alpha \tag{A.8}$$

where only the $\mathrm{U}(1)_Y$ field is shown and the $\mathrm{SU}(2)_L$ is similar. The components of $M_{5\mathrm{x}3}^{\mathrm{mix}}$ can then be obtained by calculating the following integrals:

$$-\int d^2\theta d^2\theta^\dagger \frac{m^2_{\Phi(i)}}{f_i^2}\mathbf{X}_i^\dagger\mathbf{X}_i\Phi^\dagger\Phi \to \frac{m^2_{\Phi(i)}}{f_i}v_\Phi^\dagger\tilde{\eta}_i\psi \tag{A.9}$$

$$-\int d^2\theta \frac{1}{6f_i}y^{klm}_{(i)}\mathbf{X}_i\Phi_k\Phi_l\Phi_m \to -\frac{1}{2f_i}\lambda A_{\lambda(i)}v_{\Psi_l}v_{\Psi_m}\tilde{\eta}_i\psi_k \text{ (for } \Phi_k \neq \Phi_l \neq \Phi_m) \tag{A.10}$$

$$\to \frac{1}{2f_i}\kappa A_{\kappa(i)}v_S^2\tilde{\eta}_i\tilde{S} \text{ (for } \Phi_k = \Phi_l = \Phi_m = \mathbf{S}) \tag{A.11}$$

$$-\int d^2\theta \frac{M_{B(i)}}{2f_i}\mathbf{X}_i\mathbf{W}\mathbf{W} \to \frac{M_{B(i)}}{\sqrt{2}f_i}D_Y\tilde{\eta}_i\tilde{B} \tag{A.12}$$

where Φ is a general chiral superfield like equation (2.17) that can be $\Phi = \mathbf{H}_d, \mathbf{H}_u, \mathbf{S}$ with v_Φ the VEV of the scalar part in Φ and ψ the supermultiplet part of the superfield. y^{klm} is the Yukawa coupling matrix which is symmetric under interchange of i, j and k and the Yukawa coupling of a fermion with a gaugino and a scalar is governed by the gauge coupling [22]. The mixing component of the wino is analogous to the one of the bino and $D_Y = -g_1 v^2 \cos 2\beta/2$ and $D_{T^3} = g_2 v^2 \cos 2\beta/2$. On the RHS the mixing terms are written that follow from the integrals, where only the mixing terms of order $\frac{1}{f_i}$ are written and thus the soft mass terms are left out and terms of order $\frac{1}{f_i^2}$ or higher are neglected. This results in the $M_{5\mathrm{x}3}^{\mathrm{mix}}$ in equation (2.29).

Appendix B

Parameters and definitions

The following definitions of parameters have been used:

$$
\begin{aligned}
g_1 &= \frac{2 \sin\theta m_Z}{v} \\
g_2 &= \frac{2 \cos\theta m_Z}{v} \\
v_d &= v \cos\beta \\
v_u &= v \sin\beta \\
v &= \frac{1}{\sqrt{\sqrt{2} G_f}} \\
D_Y &= -\frac{g_1 v^2 \cos^2\beta}{4} \\
D_{T^3} &= \frac{g_2 v^2 \cos^2\beta}{4} \\
cos\theta &= \frac{m_W}{m_Z}
\end{aligned}
$$

From the integrals in section 2.3.1 the parameters in the matrix $\mathcal{M}_{\tilde{\chi}^0}$ can be derived from the tadpole equations:

$$m_{H_d}^2 = -\frac{-\frac{1}{\sqrt{2}}\lambda A_\lambda v_u v_s + \frac{1}{8}(g_1^2+g_2^2)v_d(v_d^2-v_u^2) + \frac{1}{2}\lambda^2 v_d(v_u^2+v_s^2) - \frac{1}{2}\lambda\kappa v_u v_s^2}{v_d}$$

$$m_{H_u}^2 = -\frac{-\frac{1}{\sqrt{2}}\lambda A_\lambda v_d v_s - \frac{1}{8}(g_1^2+g_2^2)v_u(v_d^2-v_u^2) + \frac{1}{2}\lambda^2 v_u(v_d^2+v_s^2) - \frac{1}{2}\lambda\kappa v_d v_s^2}{v_u}$$

$$m_S^2 = -\frac{-\frac{1}{\sqrt{2}}\lambda A_\lambda v_d v_u + \frac{1}{\sqrt{2}}\kappa A_\kappa v_s^2 + \frac{1}{2}\lambda^2 v_s(v_d^2+v_u^2) + \kappa^2 v_s^2 - \lambda\kappa v_d v_u v_s}{v_s}$$

Appendix C

Event count per selection criterion per background

	Event count						
Background	after skimming	preselection	$\gamma_3\ p_{\mathrm{T}} > 85$	$\gamma_2\ p_{\mathrm{T}} > 105$	$\gamma_1\ p_{\mathrm{T}} > 105$	$E_{\mathrm{T}}^{\mathrm{miss}} > 80$	SR
γj	23415532	18907	2	2	2	0	0
$Z\gamma$	8968593	4865	5	3	3	1	1
$W\gamma$	2241409	3632	1	1	1	1	1
$W\gamma\gamma$	18508	3656	5	5	5	1	1
$Z\gamma\gamma$	25355	4504	5	4	4	0	0
$\gamma\gamma\gamma$	2662	556	15	11	11	0	0
Total	**35833436**	**36120**	**33**	**26**	**26**	**3**	**3**

Table C.1: The event count per background group for each selection criterion.

Appendix D

Background samples

Listed below are the names of the background MC samples used in this thesis.

γj

mc16_13TeV.361039.Sherpa_CT10_SinglePhotonPt35_70_CVetoBVeto.deriv.DAOD_SUSY12.e3587_s3126_r9364_p3652
mc16_13TeV.361040.Sherpa_CT10_SinglePhotonPt35_70_CFilterBVeto.deriv.DAOD_SUSY12.e3587_s3126_r9364_p3652
mc16_13TeV.361041.Sherpa_CT10_SinglePhotonPt35_70_BFilter.deriv.DAOD_SUSY12.e3587_s3126_r9364_p3652
mc16_13TeV.361042.Sherpa_CT10_SinglePhotonPt70_140_CVetoBVeto.deriv.DAOD_SUSY12.e3587_s3126_r9364_p3652
mc16_13TeV.361043.Sherpa_CT10_SinglePhotonPt70_140_CFilterBVeto.deriv.DAOD_SUSY12.e3587_s3126_r9364_p3652
mc16_13TeV.361044.Sherpa_CT10_SinglePhotonPt70_140_BFilter.deriv.DAOD_SUSY12.e3587_s3126_r9364_p3652
mc16_13TeV.361045.Sherpa_CT10_SinglePhotonPt140_280_CVetoBVeto.deriv.DAOD_SUSY12.e3587_s3126_r9364_p3652
mc16_13TeV.361046.Sherpa_CT10_SinglePhotonPt140_280_CFilterBVeto.deriv.DAOD_SUSY12.e3587_s3126_r9364_p3652
mc16_13TeV.361047.Sherpa_CT10_SinglePhotonPt140_280_BFilter.deriv.DAOD_SUSY12.e3587_s3126_r9364_p3652
mc16_13TeV.361048.Sherpa_CT10_SinglePhotonPt280_500_CVetoBVeto.deriv.DAOD_SUSY12.e3587_s3126_r9364_p3652
mc16_13TeV.361049.Sherpa_CT10_SinglePhotonPt280_500_CFilterBVeto.deriv.DAOD_SUSY12.e3587_s3126_r9364_p3652
mc16_13TeV.361050.Sherpa_CT10_SinglePhotonPt280_500_BFilter.deriv.DAOD_SUSY12.e3587_s3126_r9364_p3652
mc16_13TeV.361051.Sherpa_CT10_SinglePhotonPt500_1000_CVetoBVeto.deriv.DAOD_SUSY12.e3587_s3126_r9364_p3652
mc16_13TeV.361052.Sherpa_CT10_SinglePhotonPt500_1000_CFilterBVeto.deriv.DAOD_SUSY12.e3587_s3126_r9364_p3652
mc16_13TeV.361053.Sherpa_CT10_SinglePhotonPt500_1000_BFilter.deriv.DAOD_SUSY12.e3587_s3126_r9364_p3652
mc16_13TeV.361054.Sherpa_CT10_SinglePhotonPt1000_2000_CVetoBVeto.deriv.DAOD_SUSY12.e3587_s3126_r9364_p3652
mc16_13TeV.361055.Sherpa_CT10_SinglePhotonPt1000_2000_CFilterBVeto.deriv.DAOD_SUSY12.e3587_s3126_r9364_p3652
mc16_13TeV.361056.Sherpa_CT10_SinglePhotonPt1000_2000_BFilter.deriv.DAOD_SUSY12.e3587_s3126_r9364_p3652
mc16_13TeV.361057.Sherpa_CT10_SinglePhotonPt2000_4000_CVetoBVeto.deriv.DAOD_SUSY12.e3587_s3126_r9364_p3652
mc16_13TeV.361058.Sherpa_CT10_SinglePhotonPt2000_4000_CFilterBVeto.deriv.DAOD_SUSY12.e3587_s3126_r9364_p3652
mc16_13TeV.361059.Sherpa_CT10_SinglePhotonPt2000_4000_BFilter.deriv.DAOD_SUSY12.e3587_s3126_r9364_p3652
mc16_13TeV.361060.Sherpa_CT10_SinglePhotonPt4000_CVetoBVeto.deriv.DAOD_SUSY12.e3587_s3126_r9364_p36521
mc16_13TeV.361061.Sherpa_CT10_SinglePhotonPt4000_CFilterBVeto.deriv.DAOD_SUSY12.e3587_s3126_r9364_p3652
mc16_13TeV.361062.Sherpa_CT10_SinglePhotonPt4000_BFilter.deriv.DAOD_SUSY12.e3587_s3126_r9364_p3652

$Z\gamma$

mc16_13TeV.364500.Sherpa_222_NNPDF30NNLO_eegamma_pty_7_15.deriv.DAOD_SUSY12.e5928_s3126_r9364_p3652
mc16_13TeV.364501.Sherpa_222_NNPDF30NNLO_eegamma_pty_15_35.deriv.DAOD_SUSY12.e5928_s3126_r9364_p3652
mc16_13TeV.364502.Sherpa_222_NNPDF30NNLO_eegamma_pty_35_70.deriv.DAOD_SUSY1.e5928_s3126_r9364_p3703/
mc16_13TeV.364503.Sherpa_222_NNPDF30NNLO_eegamma_pty_70_140.deriv.DAOD_SUSY1.e5928_e5984_s3126_r10724_r10726_p3990
mc16_13TeV.364504.Sherpa_222_NNPDF30NNLO_eegamma_pty_140_E_CMS.deriv.DAOD_SUSY1.e5928_s3126_r10201_p3990
mc16_13TeV.364505.Sherpa_222_NNPDF30NNLO_mumugamma_pty_7_15.deriv.DAOD_SUSY1.e5928_s3126_r9364_p3703
mc16_13TeV.364506.Sherpa_222_NNPDF30NNLO_mumugamma_pty_15_35.deriv.DAOD_SUSY12.e5988_s3126_r9364_p3652
mc16_13TeV.364507.Sherpa_222_NNPDF30NNLO_mumugamma_pty_35_70.deriv.DAOD_SUSY1.e5928_s3126_r9364_p3703
mc16_13TeV.364508.Sherpa_222_NNPDF30NNLO_mumugamma_pty_70_140.deriv.DAOD_SUSY1.e5928_s3126_r10201_p3990
mc16_13TeV.364509.Sherpa_222_NNPDF30NNLO_mumugamma_pty_140_E_CMS.deriv.DAOD_SUSY1.e5928_s3126_r10201_p3990
mc16_13TeV.364510.Sherpa_222_NNPDF30NNLO_tautaugamma_pty_7_15.deriv.DAOD_SUSY12.e5928_e5984_s3126_r10201_r10210_p3652
mc16_13TeV.364511.Sherpa_222_NNPDF30NNLO_tautaugamma_pty_15_35.deriv.DAOD_SUSY1.e5928_s3126_r9364_p3703
mc16_13TeV.364512.Sherpa_222_NNPDF30NNLO_tautaugamma_pty_35_70.deriv.DAOD_SUSY1.e5928_s3126_r9364_p3703
mc16_13TeV.364513.Sherpa_222_NNPDF30NNLO_tautaugamma_pty_70_140.deriv.DAOD_SUSY1.e5982_s3126_r9364_p3990
mc16_13TeV.364514.Sherpa_222_NNPDF30NNLO_tautaugamma_pty_140_E_CMS.deriv.DAOD_SUSY1.e5928_s3126_r10724_p3990
mc16_13TeV.364517.Sherpa_222_NNPDF30NNLO_nunugamma_pty_35_70.deriv.DAOD_SUSY1.e5928_s3126_r9364_p3703
mc16_13TeV.364518.Sherpa_222_NNPDF30NNLO_nunugamma_pty_70_140.deriv.DAOD_SUSY1.e5928_s3126_r9364_p3990
mc16_13TeV.364519.Sherpa_222_NNPDF30NNLO_nunugamma_pty_140_E_CMS.deriv.DAOD_SUSY1.e5928_s3126_r10201_p3990

$W\gamma$

mc16_13TeV364521.Sherpa_222_NNPDF30NNLO_enugamma_pty_7_15.deriv.DAOD_SUSY12.e5928_e5984_s3126_r10201_r10210_p3652
mc16_13TeV.364522.Sherpa_222_NNPDF30NNLO_enugamma_pty_15_35.deriv.DAOD_SUSY12.e5928_e5984_s3126_r10724_r10726_p3759
mc16_13TeV.364523.Sherpa_222_NNPDF30NNLO_enugamma_pty_35_70.deriv.DAOD_SUSY1.e5928_e5984_s3126_r10201_r10210_p3793
mc16_13TeV.364524.Sherpa_222_NNPDF30NNLO_enugamma_pty_70_140.deriv.DAOD_SUSY1.e5928_e5984_s3126_r10724_r10726_p3990
mc16_13TeV.364525.Sherpa_222_NNPDF30NNLO_enugamma_pty_140_E_CMS.deriv.DAOD_SUSY1.e5928_e5984_s3126_r10724_r10726_p3990
mc16_13TeV.364526.Sherpa_222_NNPDF30NNLO_munugamma_pty_7_15.deriv.DAOD_SUSY12.e5928_e5984_s3126_r10201_r10210_p3652

mc16_13TeV.364527.Sherpa_222_NNPDF30NNLO_munugamma_pty_15_35.deriv.DAOD_SUSY12.e5928_e5984_s3126_r10201_r10210_p3652
mc16_13TeV.364528.Sherpa_222_NNPDF30NNLO_munugamma_pty_35_70.deriv.DAOD_SUSY1.e5928_e5984_s3126_r10201_r10210_p3793
mc16_13TeV.364529.Sherpa_222_NNPDF30NNLO_munugamma_pty_70_140.deriv.DAOD_SUSY1.e5928_e5984_s3126_r10724_r10726_p3990
mc16_13TeV.364530.Sherpa_222_NNPDF30NNLO_munugamma_pty_140_E_CMS.deriv.DAOD_SUSY1.e5928_e5984_s3126_r10724_r10726_p399
mc16_13TeV.364531.Sherpa_222_NNPDF30NNLO_taunugamma_pty_7_15.deriv.DAOD_SUSY12.e5928_e5984_s3126_r10201_r10210_p3652
mc16_13TeV.364532.Sherpa_222_NNPDF30NNLO_taunugamma_pty_15_35.deriv.DAOD_SUSY12.e5928_e5984_s3126_r10201_r10210_p3652
mc16_13TeV.364533.Sherpa_222_NNPDF30NNLO_taunugamma_pty_35_70.deriv.DAOD_SUSY1.e5928_s3126_r10201_p3793
mc16_13TeV.364534.Sherpa_222_NNPDF30NNLO_taunugamma_pty_70_140.deriv.DAOD_SUSY1.e5928_e5984_s3126_r10724_r10726_p3990
mc16_13TeV.364535.Sherpa_222_NNPDF30NNLO_taunugamma_pty_140_E_CMS.deriv.DAOD_SUSY1.e5928_e5984_s3126_r10724_r10726_p399

$W\gamma\gamma$

mc16_13TeV.407022.Sherpa_CT10_enugammagammaPt50GeV.deriv.DAOD_SUSY1.e4000_s3126_r9364_r9315_p3703
mc16_13TeV.407023.Sherpa_CT10_munugammagammaPt50GeV.deriv.DAOD_SUSY1.e4000_s3126_r10201_p3703
mc16_13TeV.407024.Sherpa_CT10_taunugammagammaPt50GeV.deriv.DAOD_SUSY1.e4000_s3126_r10201_p3703

$Z\gamma\gamma$

mc16_13TeV.407025.Sherpa_CT10_ZeegammagammaPt50GeV.deriv.DAOD_SUSY1.e3992_s3126_r9364_p3703
mc16_13TeV.407026.Sherpa_CT10_ZmumugammagammaPt50GeV.deriv.DAOD_SUSY1.e3992_s3126_r9364_p3703
mc16_13TeV.407027.Sherpa_CT10_ZtautaugammagammaPt50GeV.deriv.DAOD_SUSY1.e3992_s3126_r9364_r9315_p3703
mc16_13TeV.407028.Sherpa_CT10_ZnunugammagammaPt50GeV.deriv.DAOD_SUSY1.e3992_s3126_r9364_p3703

$\gamma\gamma\gamma$

mc16_13TeV.407318.MGPy8EG_A14N23LO_3photons.deriv.DAOD_SUSY1.e5820_e5984_s3126_r10724_r10726_p4164

Bibliography

[1] Stephen P. Martin. A Supersymmetry primer. hep-ph/9709356.

[2] CERN. The Large Hadron Collider. `https://home.cern/science/accelerators/large-hadron-collider`.

[3] Daniel Z. Freedman, P. van Nieuwenhuizen, and S. Ferrara. Progress toward a theory of supergravity. *Phys. Rev. D*, 13:3214–3218, 1976.

[4] P.A. Zyla et al. (Particle Data Group). Review of Particle Physics. *Progr. Theor. Exper. Phys*, 2020. 083C01 (2020).

[5] The ATLAS Collaboration. Observation of a new particle in the search for the Standard Model Higgs boson with the ATLAS detector at the LHC. *Phys. Lett.*, B716:1–29, 2012.

[6] The CMS Collaboration. The CMS experiment at the CERN LHC. *J. Instrum.*, 3(08):S08004, 2008.

[7] Máximo Bañados and Ignacio A. Reyes. A short review on Noether's theorems, gauge symmetries and boundary terms. *Int. J. Mod. Phys. D*, 25(10):1630021, 2016.

[8] Jeffrey Goldstone, Abdus Salam, and Steven Weinberg. Broken Symmetries. *Phys. Rev.*, 127:965–970, 1962.

[9] F. Englert and R. Brout. Broken Symmetry and the Mass of Gauge Vector Mesons. *Phys. Rev. Lett.*, 13:321–323, 1964.

[10] Peter W. Higgs. Broken Symmetries and the Masses of Gauge Bosons. *Phys. Rev. Lett.*, 13:508–509, 1964.

[11] G. S. Guralnik, C. R. Hagen, and T. W. B. Kibble. Global Conservation Laws and Massless Particles. *Phys. Rev. Lett.*, 13:585–587, 1964.

[12] Laurent Canetti, Marco Drewes, and Mikhail Shaposhnikov. Matter and Antimatter in the Universe. *New J. Phys.*, 14:095012, 2012.

[13] Horatiu Nastase. Introduction to supergravity. 2011. arXiv:1112.3502.

[14] Y. Shadmi. Introduction to Supersymmetry. 2017. arXiv:1708.00772.

[15] Kazunari Shima and Motomu Tsuda. On Wess-Zumino gauge. *Phys. Lett. B*, 666:410–414, 2008.

[16] Gabriele Ferretti, Alberto Mariotti, Kentarou Mawatari, and Christoffer Petersson. Multiphoton signatures of goldstini at the LHC. *JHEP*, 04:126, 2014.

[17] G.F. Giudice and R. Rattazzi. Theories with gauge mediated supersymmetry breaking. *Phys. Rept.*, 322:419–499, 1999.

[18] Koichi Hamaguchi, Kazunori Nakayama, and Norimi Yokozaki. NMSSM in gauge-mediated SUSY breaking without domain wall problem. *Phys. Lett. B*, 708:100–106, 2012.

[19] Edward Witten. Dynamical breaking of Supersymmetry. *Nucl. Phys. B*, 188(3):513 – 554, 1981.

[20] Patrick Draper, Patrick Meade, Matthew Reece, and David Shih. Implications of a 125 GeV Higgs for the MSSM and Low-Scale SUSY Breaking. *Phys. Rev. D*, 85:095007, 2012.

[21] Ulrich Ellwanger, Cyril Hugonie, and Ana M. Teixeira. The Next-to-Minimal Supersymmetric Standard Model. *Phys. Rept.*, 496:1–77, 2010.

[22] M. Maniatis. The Next-to-Minimal Supersymmetric Extension of the Standard Model Reviewed. *Int. J. Mod. Phys. A*, 25, 2010.

[23] Christoffer Petersson, Alberto Romagnoni, and Riccardo Torre. Higgs Decay with Monophoton + MET Signature from Low Scale Supersymmetry Breaking. *JHEP*, 10:016, 2012.

[24] J. Ellis, J. F. Gunion, H. E. Haber, L. Roszkowski, and F. Zwirner. Higgs bosons in a nonminimal supersymmetric model. *Phys. Rev. D*, 39:844–869, 1989.

[25] Jinrui Huang, Tao Liu, Lian-Tao Wang, and Felix Yu. Supersymmetric Exotic Decays of the 125 GeV Higgs Boson. *Phys. Rev. Lett.*, 112:221803, 2014.

[26] Riccardo Argurio, Zohar Komargodski, and Alberto Mariotti. Pseudo-Goldstini in Field Theory. *Phys. Rev. Lett.*, 107:061601, 2011.

[27] Riccardo Argurio, Karen De Causmaecker, Gabriele Ferretti, Alberto Mariotti, Kentarou Mawatari, and Yoshitaro Takaesu. Collider signatures of goldstini in gauge mediation. *JHEP*, 06:096, 2012.

[28] Tao Liu, Lin Wang, and Jin Min Yang. Higgs decay to goldstini and its observability at the LHC. *Phys. Lett. B*, 726:228–233, 2013.

[29] Wolfram Research, Inc. Mathematica, Version 12.1. Champaign, IL, 2020.

[30] Koichi Funakubo and Shuichiro Tao. The Higgs sector in the next-to-MSSM. *Prog. Theor. Phys.*, 113:821–842, 2005.

[31] J. Alwall, R. Frederix, S. Frixione, V. Hirschi, F. Maltoni, O. Mattelaer, H. S. Shao, T. Stelzer, P. Torrielli, and M. Zaro. The automated computation of tree-level and next-to-leading order differential cross sections, and their matching to parton shower simulations. *JHEP*, 07:079, 2014.

[32] Joshua Ellis. TikZ-Feynman: Feynman diagrams with TikZ. *Comput. Phys. Commun.*, 210:103–123, 2017.

[33] The ATLAS Collaboration. The ATLAS Experiment at the CERN Large Hadron Collider. *J. Instrum.*, 3(08):S08003, 2008.

[34] The LHCb Collaboration. The LHCb Detector at the LHC. *J. Instrum.*, 3(08):S08005, 2008.

[35] Lyndon R Evans and Philip Bryant. LHC Machine. *J. Instrum.*, 3:S08001. 164 p, 2008. This report is an abridged version of the LHC Design Report (CERN-2004-003).

[36] S. Agostinelli and J. Allison et al. Geant4-a simulation toolkit. *Nucl. Instrum. Meth. A*, 506(3):250–303, 2003.

[37] Jovan Mitrevski. Preparing ATLAS reconstruction software for LHCs Run 2. *J. Phys.: Conf. Series*, 664(7):072034, 2015.

[38] R. Brun and F. Rademakers. ROOT: An object oriented data analysis framework. *Nucl. Instrum. Meth. A*, 389:81–86, 1997.

[39] The ATLAS Collaboration. Search for photonic signatures of gauge-mediated supersymmetry in 13 TeV pp collisions with the ATLAS detector. *Phys. Rev. D*, 97(092006), 2018.

[40] The ATLAS Collaboration. Expected photon performance in the ATLAS experiment. ATL-PHYS-PUB-2011-007, 2011.

[41] The ATLAS Collaboration. Measurement of the photon identification efficiencies with the ATLAS detector using LHC Run-1 data. *Eur. Phys. J. C*, 76(12):666.

[42] The ATLAS Collaboration. Electron efficiency measurements with the ATLAS detector using 2012 LHC proton–proton collision data. *Eur. Phys. J. C*, 77(3):195, 2017.

[43] The ATLAS Collaboration. Electron and photon energy calibration with the ATLAS detector using LHC Run 1 data. *Eur. Phys. J. C*, 74(10):3071, 2014.

[44] The ATLAS Collaboration. Electron efficiency measurements with the ATLAS detector using the 2015 LHC proton-proton collision data. ATLAS-CONF-2016-024, 2016.

[45] The ATLAS Collaboration. Muon reconstruction performance of the ATLAS detector in proton–proton collision data at $\sqrt{s}$ =13 TeV. *Eur. Phys. J. C*, 76(5):292, 2016.

[46] The ATLAS Collaboration. Tagging and suppression of pileup jets with the ATLAS detector. ATLAS-CONF-2014-018, 2014.

[47] Adam Alloul, Neil D. Christensen, Céline Degrande, Claude Duhr, and Benjamin Fuks. FeynRules 2.0 - A complete toolbox for tree-level phenomenology. *Comput. Phys. Commun.*, 185:2250–2300, 2014.

[48] J. Alwall, R. Frederix, S. Frixione, V. Hirschi, F. Maltoni, O. Mattelaer, H. S. Shao, T. Stelzer, P. Torrielli, and M. Zaro. The automated computation of tree-level and next-to-leading order differential cross sections, and their matching to parton shower simulations. *JHEP*, 07:079, 2014.

[49] Torbjorn Sjostrand, Stephen Mrenna, and Peter Z. Skands. A Brief Introduction to PYTHIA 8.1. *Comput. Phys. Commun.*, 178:852–867, 2008.

[50] Torbjorn Sjostrand, Stephen Mrenna, and Peter Z. Skands. PYTHIA 6.4 Physics and Manual. *JHEP*, 05:026, 2006.

[51] Eric Conte, Benjamin Fuks, and Guillaume Serret. MadAnalysis 5, A User-Friendly Framework for Collider Phenomenology. *Comput. Phys. Commun.*, 184:222–256, 2013.

[52] Robert D. Cousins, James T. Linnemann, and Jordan Tucker. Evaluation of three methods for calculating statistical significance when incorporating a systematic uncertainty into a test of the background-only hypothesis for a Poisson process. *Nucl. Instrum. Meth. A*, 595(2):480 – 501, 2008.